Protein Science (1992), *1*, 472-493. Cambridge University Press. Printed in the USA.

The molecular mechanism for the tetrameric association of glycogen phosphorylase promoted by protein phosphorylation

D. BARFORD[1] AND L.N. JOHNSON

Laboratory of Molecular Biophysics, University of Oxford, Rex Richards Building, South Parks Road, Oxford OX1 3QU, UK

(RECEIVED September 11, 1991; REVISED MANUSCRIPT RECEIVED December 10, 1991)

Abstract

The allosteric transition of glycogen phosphorylase promoted by protein phosphorylation is accompanied by the association of a pair of functional dimers to form a tetramer. The conformational changes within the dimer that lead to the creation of a protein recognition surface have been analyzed from a comparison of the crystal structures of T-state dimeric phosphorylase *b* and R-state tetrameric phosphorylase *a*. Regions of the structure that participate in the tetramer interface are situated within structural subdomains. These include the glycogen storage subdomain, the C-terminal subdomain and the tower helix. The subdomains undergo concerted conformational transitions on conversion from the T to the R state (overall r.m.s. shifts between 1 and 1.7 Å) and, together with the quaternary conformational change within the functional dimer, create the tetramer interface. The glycogen storage subdomain and the C-terminal subdomain are distinct from those regions that contribute to the dimer interface, but shifts in the subdomains are correlated with the allosteric transitions that are mediated by the dimer interface. The structural properties of the tetramer interface are atypical of an oligomeric protein interface and are more similar to protein recognition surfaces observed in protease inhibitors and antibody-protein antigen complexes. There is a preponderance of polar and charged residues at the tetramer interface and a high number of H-bonds per surface area (one H-bond per 130 Å^2). In addition, the surface area made inaccessible at the interface is relatively small (1,142 Å^2 per subunit on dimer to tetramer association compared with 2,217 Å^2 per subunit on monomer-to-dimer association).

Keywords: conformational changes; glycogen phosphorylase; oligomerization; phosphorylation; protein association

Regulation of protein activity and function is frequently mediated through protein-protein interactions and by changes in the state of protein oligomerization. Transmembrane signal transduction by membrane-associated receptors, exemplified by the insulin, epidermal growth factor, and colony-stimulating factor receptors, is caused by a stimulation of the intracellular tyrosine kinase domain promoted by ligand binding to the extracellular domain and is accompanied by protein association (reviewed by Yarden & Ullrich, 1988). Proteins of the G-coupled receptor system are also regulated as a consequence of changes in protein-protein interactions (reviewed by Weiss et al., 1988). The mechanisms by which oligomerization exert changes in function are unknown, although it is likely that changes in the tertiary structure of the protein accompany changes in oligomerization. Clues to how tertiary structure is dependent on quaternary structure have been obtained from studies on various allosteric proteins, for example hemoglobin (Perutz, 1987), aspartate transcarbamylase (Kantrowitz & Lipscomb, 1988), glycogen phosphorylase (Barford & Johnson, 1989), and phosphofructokinase (Schirmer & Evans, 1990). These studies have shown that transmission of signals between remote ligand-binding sites, within or between subunits, depends on the interdependence of quaternary and ter-

Reprint requests to: L.N. Johnson, Laboratory of Molecular Biophysics, University of Oxford, Rex Richards Building, South Parks Road, Oxford, OX1 3QU, UK.

[1] Present address: Cold Spring Harbor Laboratory, P.O. Box 100, Cold Spring Harbor, New York 11724.

Abbreviations: GP*a*, glycogen phosphorylase *a*; GP*b*, glycogen phosphorylase *b*; Glc-1-P, α-D-glucose-1-phosphate; superscripts: ′ denotes residues related across the *p* axis, ″ denotes residues related across the *q* axis, and ‴ denotes residues related across the *r* axis; r.m.s., root mean square; *R*-factor, $\Sigma_h |F_o - F_c| / \Sigma_h F_o$.

tiary structures. Glycogen phosphorylase also represents an example of a change in oligomerization associated with enzyme activation. An understanding of the nature of the relationship between protein oligomerization and the tertiary structure of glycogen phosphorylase may provide insight into the mechanism of regulation of other protein complexes.

Glycogen phosphorylase catalyzes the phosphorolytic degradation of glycogen into Glc-1-P. The activity of the enzyme is regulated by the interconversion between alternate structural states controlled by allosteric interactions and reversible phosphorylation. The T state exhibits a low affinity for substrates, whereas the R state exhibits a high affinity for substrates and allosteric activators. The nonphosphorylated form of the enzyme, GP*b*, is activated by AMP. The enzyme displays homotropic cooperativity toward binding of substrate and AMP (Buc, 1967; Black & Wang, 1968) and heterotropic cooperativity between AMP and substrates (Helmreich & Cori, 1964). Hormonal or neuronal signals stimulate kinase-catalyzed phosphorylation of serine 14. The activity of the phosphorylated form, GP*a*, is not dependent on AMP, although activity is enhanced by AMP. GP*a* binds substrates and AMP with a high level of affinity, although cooperatively. AMP-activated GP*b* displays approximately 95% of AMP-activated GP*a* activity (Madsen, 1986).

In the absence of effectors, GP*b* is a dimer in which each subunit has a relative molecular mass of 97,434. Activation by AMP or by phosphorylation produces an association of dimers to tetramers. Early work demonstrated that GP*a* had double the molecular weight of GP*b* (Keller & Cori, 1953). This was one of the first observations of a change in physical properties between the activated and nonactivated state of phosphorylase, and for some years it was assumed that the tetramerization and activation were intimately linked, a view put forward in older biochemistry textbooks. However the discoveries that association was inversely dependent upon ionic strength (Wang & Graves, 1963, 1964) and that tetramers are less active than dimers (they exhibit 12–33% of the activity of the fully active dimers [Metzger et al., 1967; Huang & Graves, 1970]) together with observations that glycogen or oligosaccharide promotes dissociation of less active tetramers to more active dimers have led to the view that the dimeric state is the active form of the enzyme. In muscle, phosphorylase is bound as the dimeric state to glycogen particles (Meyer et al., 1970). Some phosphorylases, such as the shark and the isozyme I of heart muscle (Davis et al., 1967) and the pig muscle phosphorylase (Oikonomakos et al., 1985) show less tendency to form tetramers on activation. The dramatic change in state of oligomerization that accompanies the T-to-R transition in the rabbit muscle enzyme (in the absence of glycogen) is often used as a diagnostic of the activation state such as in the comparison of IMP and AMP activation (Black & Wang, 1968), inhibition and stabilization of the T state by glucose (Wang et al., 1965; Withers et al., 1979), activation by modified cofactors (Withers et al., 1982), and activation by sulfate (Leonidas et al., 1990).

The structures of various forms of glycogen phosphorylase have been determined. High-resolution structures are available for T-state GP*b* crystallized with the weak activator IMP (Acharya et al., 1991) and T-state GP*a* crystallized in the presence of the inhibitor glucose (Sprang & Fletterick, 1979). In the crystals, both T-state forms exist as dimers, and the structures have been compared (Sprang et al., 1988). The structures of R-state GP*b* and GP*a* crystallized in the presence of 1.0 M ammonium sulfate have been determined to a resolution of 2.9 Å and the two R-state structures are closely similar (Barford & Johnson, 1989; Barford et al., 1991). High concentrations of ammonium sulfate induce R-state characteristics of phosphorylase, and, in both R-state forms, the enzyme exists as a tetramer (Engers & Madsen, 1968; Sotiroudis et al., 1978; Leonidas et al., 1990). The kinetic properties of the enzyme in the presence of ammonium sulfate have been established (Leonidas et al., 1990). Recently Sprang et al. (1991) have determined the R-state structure of GP*b* in the presence of AMP and a modified cofactor, in which the enzyme was crystallized from polyethylene glycol. In this structure as in the other R-state structures, the molecule is a tetramer. A comparison of the T- and R-state structures has provided an explanation for the enzyme's cooperative behavior on ligand binding and its regulation by allosteric effectors and reversible phosphorylation. The structural changes associated with sulfate-stimulated activation of GP*b* and phosphorylation of Ser 14, occurring in the vicinity of the allosteric sites at the dimer interface and catalytic sites, have been described previously (Sprang et al., 1988; Barford & Johnson, 1989; Barford et al., 1991). In this paper we report the structural features of the tetramer interface and the quaternary and tertiary conformational changes associated with formation of this interface. The properties of glycogen phosphorylase have been reviewed (Graves & Wang, 1972; Madsen, 1986; Johnson et al., 1989; Johnson, 1992).

Results

Description of the overall structure

The organization of secondary structure in both T and R states is similar. The subunit structure of the enzyme is composed of two domains of approximately equal size (Fig. 1). These comprise residues 10–484 (the N-terminal domain) and residues 485–842 (the C-terminal domain). (Residues 1–10 have not been located.) Each domain is centered on an α/β structure. In addition, the C-terminal domain contains a substantial amount of all α structure (residues 714–825, helices α23–α29). A diagram of the protein topology is shown in Figure 2, and a detailed

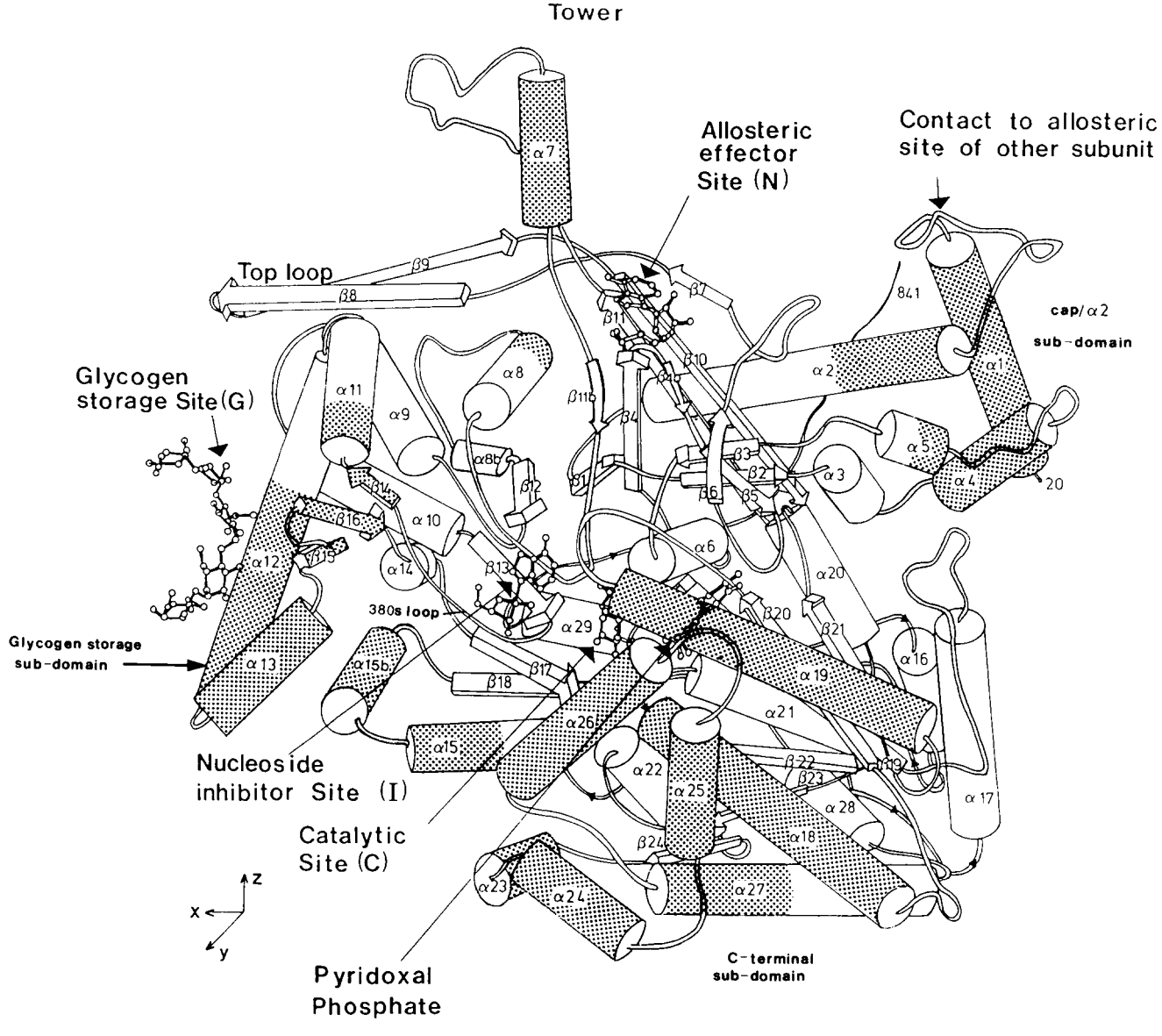

Fig. 1. Schematic diagram of T-state GP*b* (adapted from Acharya et al., 1991) viewed along the crystallographic y axis (T-state GP*b* tetragonal crystals). α-helices and β-strands are represented by cylinders and arrows, respectively. Glucose-1-phosphate and pyridoxal 5′-phosphate are shown bound to the catalytic site. Maltopentose is shown bound to the glycogen storage site (part of the glycogen storage subdomain). The C-terminal subdomain is located at the lower right of the subunit and the cap/α2 subdomain is located at the top right. Regions where Cα-atom positions differ by more than 0.5 Å between T-state GP*b* and R state GP*a* are shown as shaded (dotted) areas.

The diagram omits the first 20 residues, and the polypeptide chain begins with the α1 helix (residues 23–38) (in which an extra N-terminal turn occurs in T-state GP*b*) followed by the cap structure, a loop connecting the α1- and α2-helices. The α1-helix packs against the start of α2, with the remainder of the α2 helix packing against strands β7, β10, β11, and β4 of the central β-sheet core. Leading from α2, the polypeptide chain forms the central β-strand, β1, of the β-sheet. The chain then makes the first excursions from the central sheet with the β2-strand, which with β3 forms part of a two-stranded antiparallel β-sheet. Following β2, the chain enters a bundle of three α-helices, α3, α4, and α5. The α4 helix packs against α1, and the start of α5 is associated with the N-terminus of α2. The helices α1 and α4 and the N-termini of both α2 and α5 form a compact independent subdomain, termed the cap/α2 subdomain. The β3 strand leads into α6, which packs closely against the β-sheet core. The turn connecting β3 with α6 forms part of the catalytic site (residues 131–134). The chain then enters a mixed β-sheet formed by β5 and β6 leading into the peripheral strand of the core, β7. The β7 strand is antiparallel to β10 and joined to it via an antiparallel β-sheet formed from β8 and β9. This sheet produces the second major excursion from the core. The β11 strand, antiparallel to β10, is linked to the tower helix (residues 261–274) by a loop of flexible residues. The tower helix, which forms the most significant excursion from the core, is anchored at its base by a β-strand (β11b, residues 276–279), which is part of a mixed β-sheet including β5 and β6. The β11b strand leads into the 280s loop (residues 281–287), a hairpin loop forming a gate to the catalytic site entrance in the T state. Pro 281 is associated with Asn 133 of β3 and Ile 165 of β5. The 280s loop leads into the

(*continued on facing page*)

Table 1. *Classification of subdomains*

Name	Residues	Secondary structure	Subunit interface	Structure change T to R	Reference
N-terminal domain					
N-terminal tail	10–23	–	p axis (GP*a* only)	Yes	Barford & Johnson, 1989; Barford et al., 1991
Cap/α2	23–58	α1, cap, α2	p axis	Yes	Barford & Johnson, 1989; Barford et al., 1991
α4/α5	104–124	α4, α5			
Tower/280s loop	261–285	α7	p axis	Yes	Barford & Johnson, 1989; Barford et al., 1991
			r axis		This work
Glycogen storage	388–448 456–475	α11, α12, α13, β15, β16, α14 α15a, α15b	q axis	Yes	This work
C-terminal domain					
Structural unit 1	485–561	π, α16, 310, α17	–	No	This work
Structural unit 2	562–645	β19, α18, β20, α19, β21	q axis	Yes	This work
Structural unit 3	646–710	α20, β22, α21, β23, α22, β24	–	No	This work
Structural unit 4	711–785	α23, α24, α25, α26, α27	q axis	Yes	This work
Structural unit 5	786–837	α27, α28, α29	–	No	This work
C-terminal subdomain units 2 & 4	568–593 608–645 711–785	α18 α19/β21 α23, α24, α25, α26, α27	q axis	Yes	This work

description of T-state GP*b* is presented in Acharya et al. (1991).

Each domain has subdomains composed of compact structural folds existing independently from the main domain fold. These subdomains are of interest as they undergo conformational changes on interconversion between the T and R states and are involved in forming intersubunit contacts. The subdomains are defined in Table 1. In the N-terminal domain, the subdomains comprise excursions of the chain from the central core of the structure (see Kinemage 1). They include the N-terminal tail, the cap/α2 unit, the tower helix with the 280s loop, and the glycogen storage subdomain. In the C-terminal domain, the protein fold allows a division into five structural units (see Kinemage 2). The independent structural units are delineated by a two-dimensional distance geometry plot (Phillips, 1970) (Fig. 3). The plot represents a contour map of the interatomic distances between pairs of Cα-atoms with the lowest contour corresponding to separations of 35 Å and the highest contour to separations of

Fig. 1. *Continued*

α8 helix, which packs against the β-sheet core. Residues of the C-terminus of the α8 helix participate in producing the AMP allosteric site located at the dimer interface.

The chain then forms a mobile and irregular loop before developing into a short helix, α8b, and subsequently joining the β-sheet core at β12. At the end of β12, the chain forms α9, a helix packing closely against the β-sheet, and then into α10, before rejoining the sheet at β13. The loop connecting β13 to β14 (the 380s loop, residues 377–385) forms part of the catalytic site. The β14 strand is a strand of a mixed β-sheet also consisting of β15 and β16 with β14 connected to β15 via 3 α-helices, α11, α12, and α13. The chain then folds into a reverse turn of β15 and β16. The α12–α13 pair of helices exists autonomously except where they pack against the α15a and α15b helices. The α12, α13, and the β-strands β15 and β16 form the glycogen storage subdomain, which includes the glycogen storage site. From this subdomain, the chain leads into α14 and β17 of the central β-sheet and from there to α15a and α15b and finally to the last strand of the β-sheet, β18.

The chain enters the C-terminal domain with a compact bundle of four helices consisting of a π helix, α16, two 3_{10} helices, and α17. At the center of the C-terminal domain is the dinucleotide-binding fold consisting of a core of six parallel β-strands, β19–β24. Flanked on one face are two helices, α18 and α19, and on the opposite face of the sheet, α20, α21, and α22. The chain then folds into an α-helical region in which α-helices α23–α26 and the N-terminus of α27 form one unit and helices α27, α28, and α29 form a second unit.

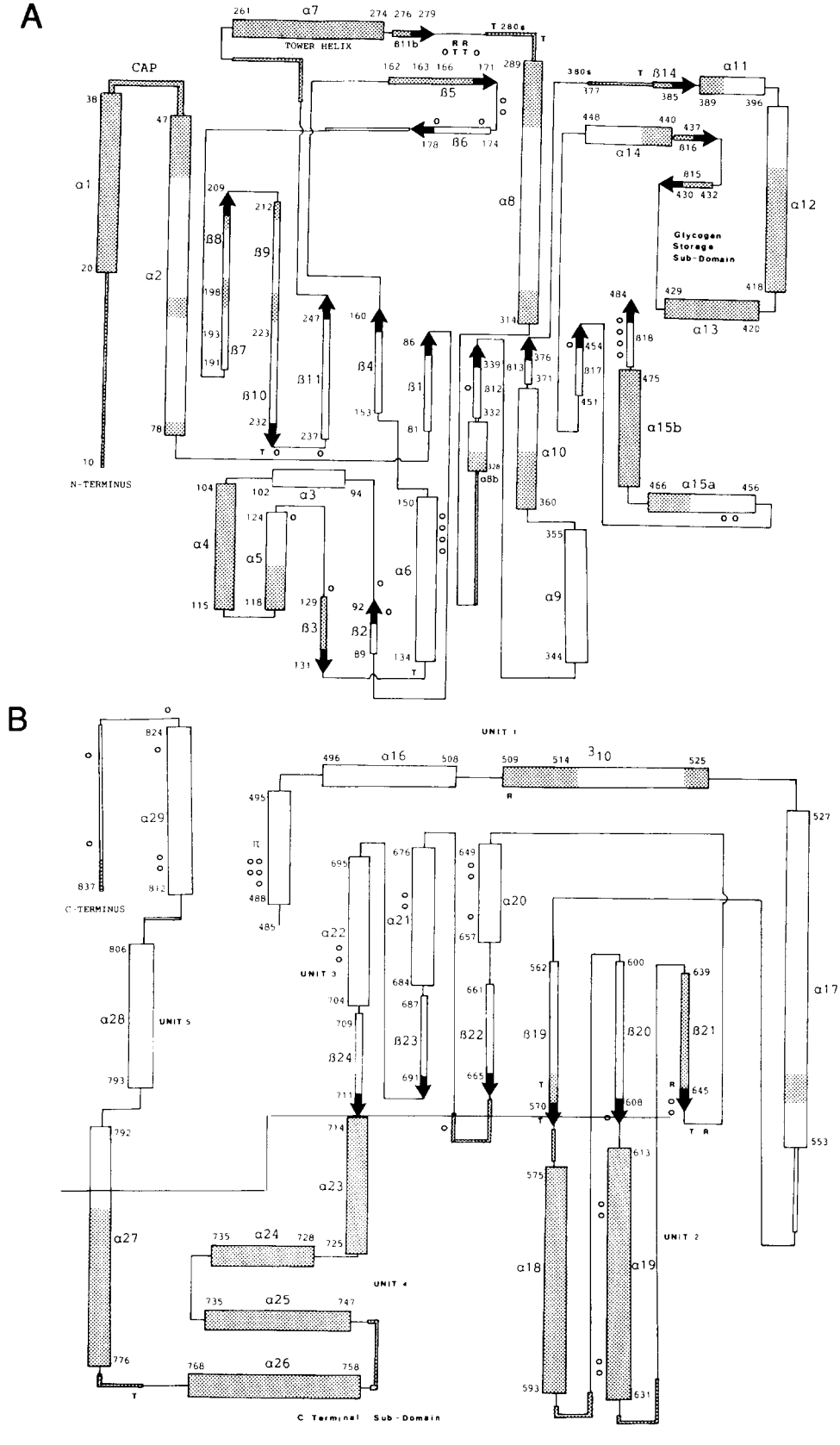

Fig. 2. Topology diagram of **(A)** N-terminal domain (residues 10–484) and **(B)** C-terminal domain (residues 485–842) of glycogen phosphorylase. Regions where Cα-atoms differ by more than 0.5 Å between T-state GP*b* and R-state GP*a* are shown shaded. The positions of interdomain H-bonds and salt bridges are indicated (O representing interactions common to both states; T, interactions unique to the T state; and R, interactions unique to the R state). The subdomains are indicated.

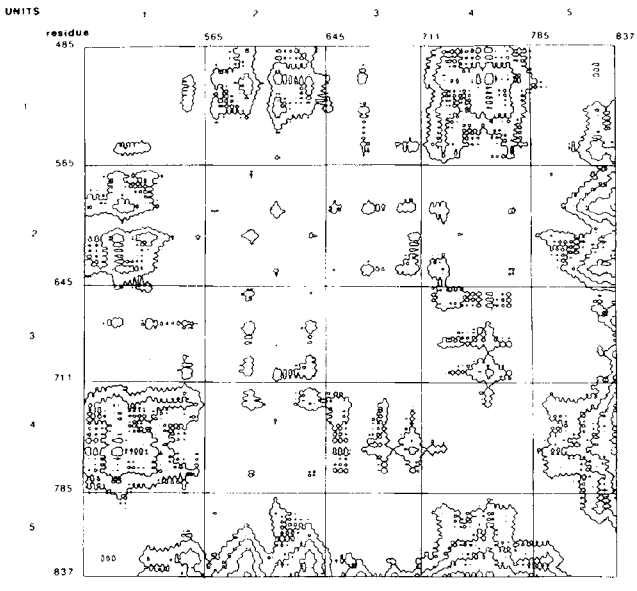

Fig. 3. Two-dimensional distance geometry plots of the C-terminal domain. Interatomic distances are contoured from 35 Å to 80 Å at intervals of 10 Å. The division of the C-terminal domain into five structural units is depicted.

80 Å. Hence, positions on the map corresponding to long-range interatomic contacts are indicated by high density and positions of short-range contact by low density. Units 1, 3, and 5 are close together in the structure, as are units 2 and 4, but units 1, 3, and 5 form few contacts to units 2 and 4. Elements of units 2 and 4 together, comprising the helices α18 and α19 and the helices α23–α27, are termed the C-terminal subdomain. Units 1, 3, and 5 and the C-terminal subdomain occupy different positions within the domain. The C-terminal subdomain is situated on the face of the β-sheet forming the catalytic surface and residues of the α23–α24 loop and α25–α26 loop participate in interdomain contacts. Units 1, 3, and 5 are located on the opposite side of the molecule that contains the allosteric and Ser-P regulatory sites (Fig. 1).

In the T-state crystal structures of GP*a* and GP*b*, the enzyme exists as a dimer. The two subunits are related by a crystallographic twofold axis of symmetry. The dimer interface between the subunits comprises contacts that are located principally at two distinct sites on the surface (Acharya et al., 1991) (Fig. 4A). One contact, the cap′/α2 interface, is formed by the association of the cap′ (a loop of residues 35–45 that connects the first and second helices α1′ and α2′) with the α2 helix and β7 strand of the opposite subunit (superscript ′ denotes regions of the structure from the symmetry-related subunit). A second contact is formed by the antiparallel association of a pair of α-helices, termed the tower helices, one from each subunit, which link the catalytic site to the subunit interface and hence indirectly to the allosteric and phosphorylation sites. On the T-to-R transition one subunit rotates with respect to the other by 10° about an axis normal to the twofold axis of the dimer, and there are major changes at the subunit contacts that include a tightening of the cap′/α2 contact and a change in the packing of the tower helices (Kinemages 4–6; Barford & Johnson, 1989). On phosphorylation or activation by sulfate, the N-terminal residues 10–23 adopt a different conformation and change their interactions from intrasubunit contacts to intersubunit contacts. The unphosphorylated Ser 14 is surrounded by acidic residues in GP*b*, and the Ser 14-P in GP*a* contacts two basic residues, Arg 69 and Arg 43′ (Sprang et al., 1988; Barford et al., 1991). The concerted changes in tertiary and quaternary structure on the T-to-R transition not only alter the structure of the dimer subunit interface but are also accompanied by changes elsewhere on the surface.

Tetramer interface contacts

In all crystal structures of the R-state enzyme the aggregation state is a tetramer, consistent with solution experiments that have shown that aggregation accompanies activation in the absence of glycogen. The crystal structure shows that functional dimers aggregate to form a square planar array with 222 symmetry (Fig. 4B; Kinemages 3, 4). The twofold axes do not correspond to crystallographic axes of symmetry, but previous analysis has shown that the subunits are identical to within the precision of the data (Barford & Johnson, 1989). The axes p, q, and r represent the three mutually orthogonal axes. The p axis corresponds to the dyad axes of the functional dimer. Within the tetramer interface, the majority of interactions are produced across the q axis, and there are relatively few contacts across the r axis.

Regions of the subunit that are involved in the tetramer contacts are shown in Figure 5. The view is down the p axis and is normal to the view shown in Figure 4. This figure shows the same view of the dimer as in Figure 1c in Barford et al. (1991), but in the present diagram those regions involved in the tetramer interface are highlighted in contrasting colors, whereas in the figure in Barford et al. those parts of the molecule that shift on the T-to-R transition are highlighted. There is a close correspondence between those regions that change in structure and those regions involved in subunit contacts. The conformational changes are described in the next section.

Across the q axis, two types of contacts exist arising from four structural elements on each subunit producing six tetramer contacts in total. One contact is produced between residues 723 and 729, a loop connecting α-helices α23 and α24 of the C-terminal subdomain, with their symmetry-related counterparts, indicated in green in Figure 5 and shown in detail in Figure 6. The contact is formed by the polar interactions of the main-chain carbonyls of residues Gln 723, Arg 724, and Gly 725 with the

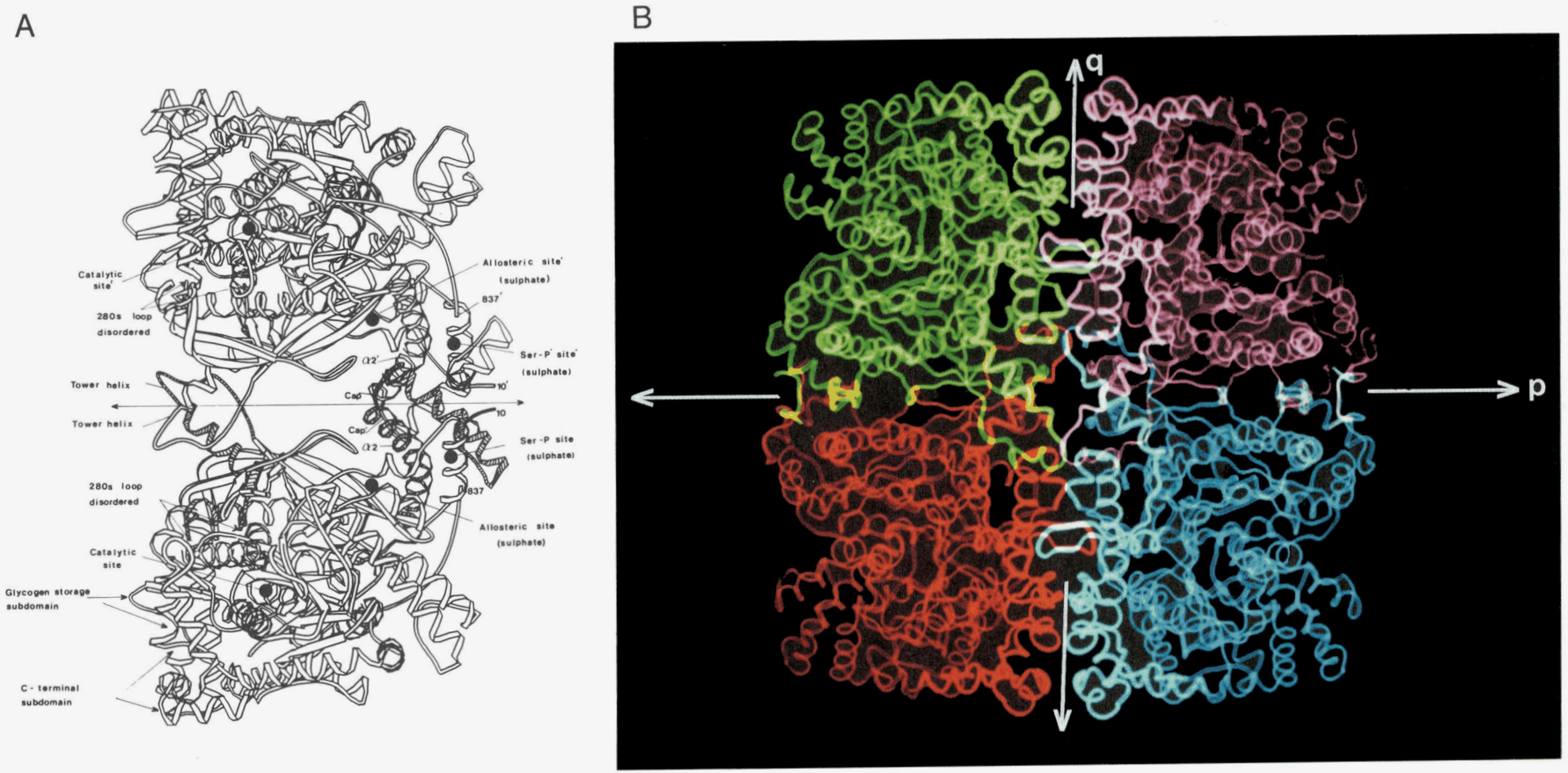

Fig. 4. Representations of the phosphorylase R-state dimer and tetramer. **A**: A ribbon diagram of the R-state dimer viewed normal to the p axis, the twofold axis of the dimer (adapted from Barford & Johnson, 1989). The view is approximately 45° from the view shown in Figure 1 . The glycogen storage subdomain and the C-terminal subdomain are indicated in addition to the catalytic, allosteric, and Ser-P sites and other important structural features. **B**: Ribbon representation of Cα-atom trace of an R-state GP*a* tetramer indicating the molecular 222 symmetry. The view is similar to A but not identical, and many of the features labeled in A can be identified in the purple/blue dimer on the right of the figure. The dimer interface (across the p axis) is horizontal, and the tetramer interface (across the q axis) is vertical. The r axis of the tetramer is normal to the page. Referring to the purple/blue dimer on the right hand side of the figure, the cap′/α2 interface is at the far right with the α2 helix viewed almost end on, and the tower/tower helix interface is on the lefthand side of the subunits with the towers emphasized in stronger colors. Referring to the blue and red subunits and their interactions across the vertical q axis of the tetramer, the helical C-terminal subdomain is highlighted in the lower part of the figure, and this subdomain partially obscures the glycogen storage subdomain, although the protruding β15/β16 loops are visible. The tower helices also interact across the q axis; the towers of the blue and red subunits interact just above the intersection of the three dyads and those of the purple and green subunits just below. Residues from the tower helices also associate across the r axis; residues from the blue subunit with those from the green subunit and those from the purple subunit with those from the red subunit. Further details are described in the text.

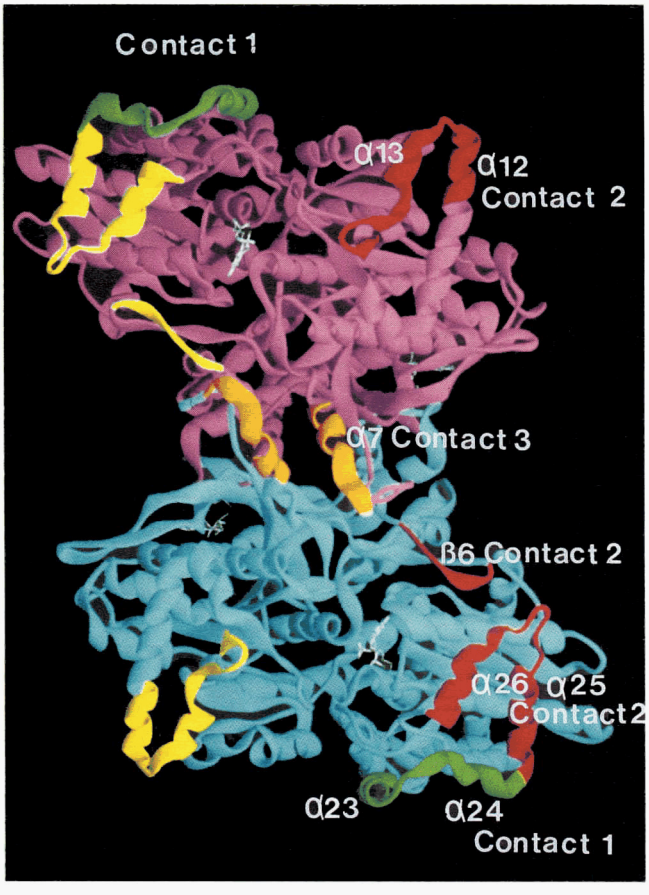

Fig. 5. Color diagram showing the location of the tetramer interface contacts. Cα-atom ribbon trace of the R-state GP*a* dimer viewed down the p-dyad axis onto the catalytic face of the molecule, i.e., 90° about the q axis from Figure 4. The q- and r-dyad axes are vertical and horizontal, respectively. Regions across the q axis that form contact 1 are colored green, and regions that form contact 2 are in red with the symmetry-related contacts in yellow. The tower helices that form interactions across all three axes (p, q, r) are indicated in orange.

Table 2. *R-state GPa tetramer interface interactions*

Hydrogen bonds and salt bridges <3.5 Å	Van der Waals contacts <4.0 Å	
q axis	q axis	
Contact 1	Contact 1	
Gln 723 O ... Gln 729 NE2	Asp 722	His 767
Arg 724 O ... Asn 727 ND2	Gln 723	Gln 729
Gly 725 O ... Asn 727 ND2	Arg 724	Asn 727
		Gln 729
	Gly 725	Asn 727
Contact 2	Contact 2	
Arg 426 NH1 ... Asp 756 OD1	Trp 174	Glu 433
... Asp 756 OD2		Gly 434
		Ala 435
Glu 433 O ... Gln 754 NE2	Asp 423	Pro 755
	Arg 426	Lys 753
		Pro 755
		Asp 756
	Glu 433	Gln 754
	Contact 3	
	Tyr 262	Ile 263
r axis	r axis	
	Tyr 262	Leu 267
None		Leu 271
	Gln 264	Gln 264
		Leu 267

side chains of Asn 727″ and Gln 729″ of the opposite subunit. There are six main-chain/side-chain H-bonds (Table 2). (The amide group of the side chain of Asn 727 was flipped 180° from the previously assigned arbitrary position in order to make these H-bonds.) A comparison of the conformation of residues at this interface with their equivalents in the T state indicates that there are no local conformational changes involving the main-chain or side-chain atoms occurring on formation of this subunit contact, but these residues are part of the C-terminal subdomain that shifts as a rigid body as described below.

A second contact comprises three regions of the structure: (1) residues 423–435 of the α13 helix and the β15/β16 sheet of the glycogen storage subdomain of one subunit to (2) residues 752″–756″, a loop connecting the α25 and α26 helices of the C-terminal subdomain and (3) Trp 174″ of β6 of the opposite subunit. The interactions formed at this interface are both ionic and polar with an H-bond formed between the side chain of Arg 426 and Asp 756″ and between the Gln 754″ side-chain to the main-chain carbonyl of Glu 433. A hydrophobic interaction is created by the association of Trp 174″ to Gly 434 and Ala 435. Details are given in Table 2 and illustrated in Figure 7. The regions of the molecule forming this contact are colored red with the symmetry-related structural elements in yellow in Figure 5. These contacts are facilitated by local side-chain conformational changes in addition to subdomain motions. The side-chain of Gln 754″ rotates by 180° to form an H-bond to the main-chain carbonyl of Glu 433, and the carboxylate group of Asp 756″ shifts by 2 Å forming a salt bridge to Arg 426. This tetramer contact is formed from part of the glycogen-binding site. Residues of β15, β16, and α13, particularly the side chains of Arg 426 and Glu 433 contribute to this site (Johnson et al., 1988, 1990).

Residues of the tower helix contribute to all three subunit interfaces. The most substantial contribution involves the dimer interface (p), which undergoes a radical conformational change during the T-to-R state transition (Barford & Johnson, 1989) (Fig. 8). In the tetramer, a nonpolar contact is formed across the r interface between the side chains of Tyr 262 and Leu 267‴ and between Gln 264 and Gln 264‴. Across the q interface Tyr 262 forms

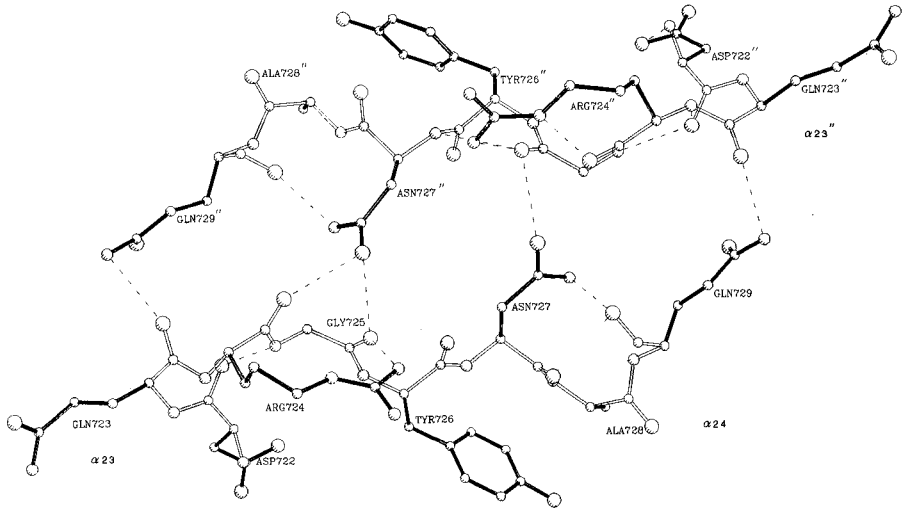

Fig. 6. Interactions at contact 1 of the q-tetramer interface. The view is down the q axis. The interactions involve association of residues from the loop between $\alpha 23$ and $\alpha 24$ about the twofold q axis with their symmetry-related residues.

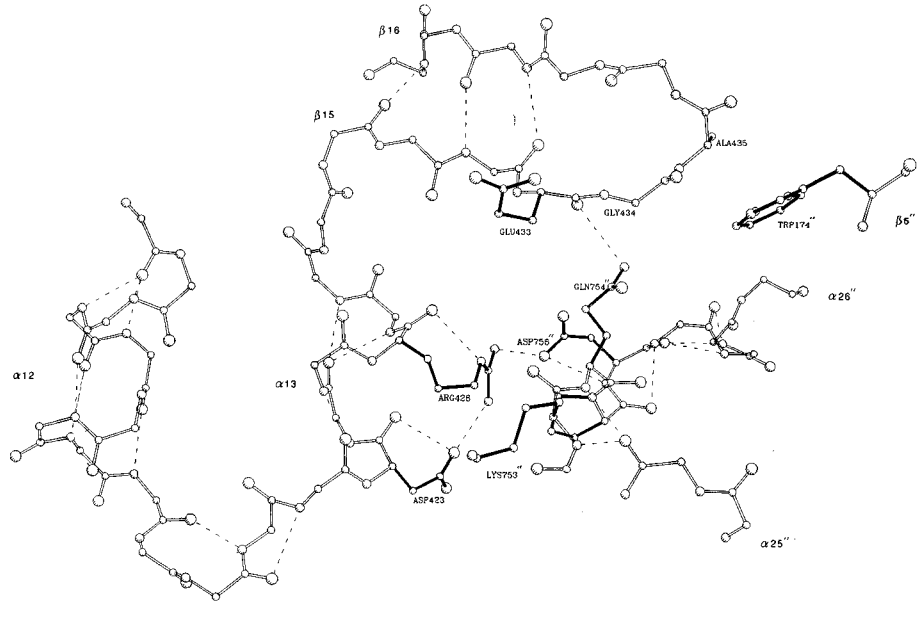

Fig. 7. Interactions at contact 2 of the q-tetramer interface. The view is normal to the q axis as in Figure 4B. Residues from the glycogen storage subdomain ($\alpha 13$ and $\beta 15$) are in contact with those from the $\alpha 25/\alpha 26$ loop.

a van der Waals interaction to Ile 263'' (Table 2). In the T state, Tyr 262 is associated with Pro 281′ in a contact across the dimer p axis, an interaction that is destroyed on the T-to-R transition, which leaves Tyr 262 exposed for other interactions.

The association of isolated R-state subunits about the p axis to form dimers results in a change of solvent-accessible area of 2,217 Å^2 per subunit. The change in solvent-accessible area on association of dimers about the q and r axes to form the the tetramer is 1,142 Å^2 per subunit in which association about the q and r interfaces buries 782 Å^2 and 360 Å^2 per subunit, respectively. Hence the total area buried per subunit on association of subunits to the tetramer is 3,359 Å^2 with 66% of this area arising from formation of the dimer interface. The tetramer interface is smaller than the dimer interface and is less than the average value for interface contact areas listed by Miller et al. (1987) in a survey of 23 protein structures. The dimer interface (p) and the tetramer interface (q and r) correspond to 7% and 3%, respectively, of the total subunit solvent-accessible area.

The contributions to the change in solvent-accessible area on formation of the tetramer are listed in Table 3. The two major contacts across the q axis (described above) contribute 156 Å^2 and 536 Å^2 per subunit for contacts 1 and 2, respectively. Thus, 68% of the change in solvent-accessible surface area on formation of tetramers occurs at the q interface, and about this axis the as-

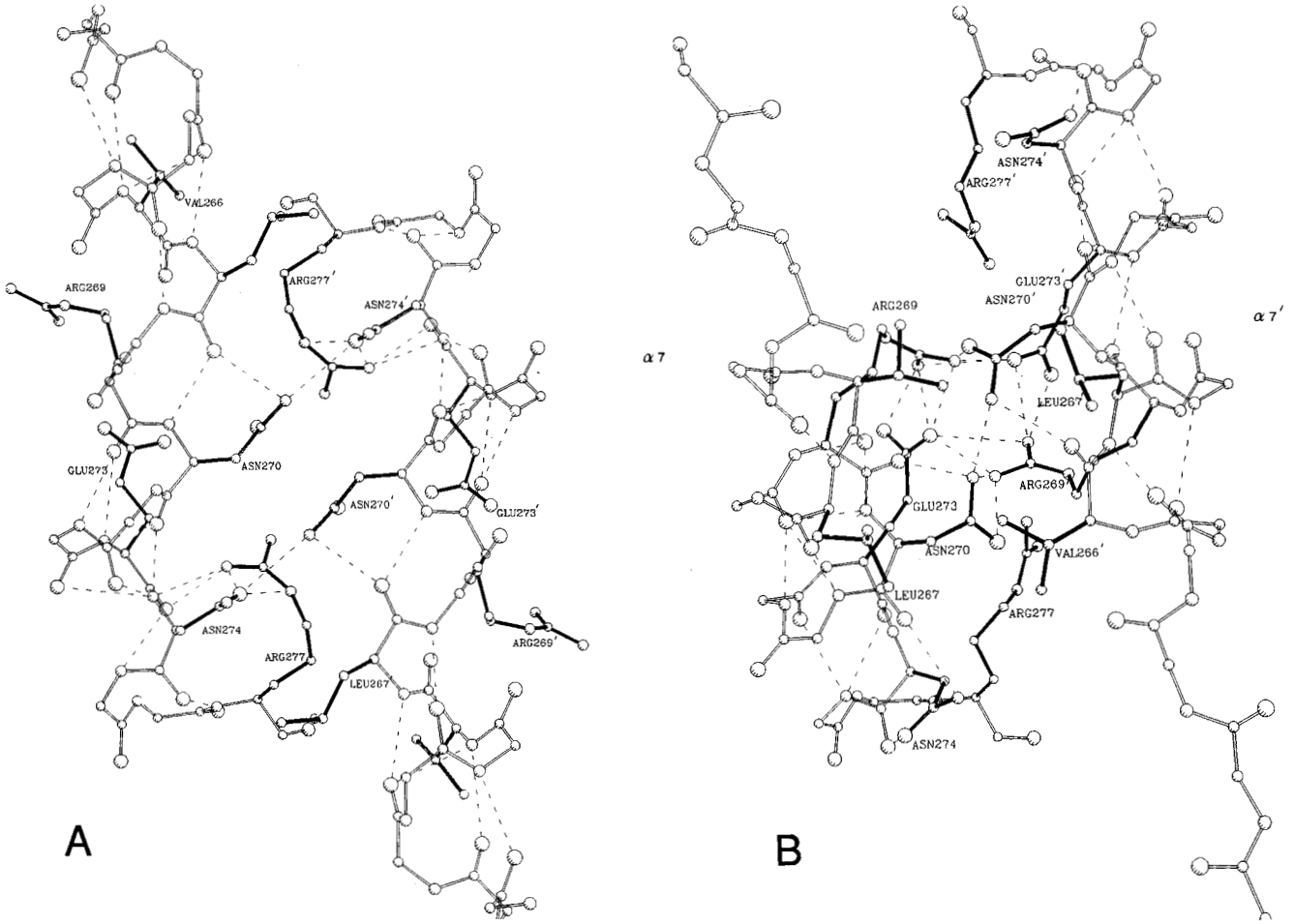

Fig. 8. Interactions at the tower helix dimer interface viewed down the molecular dyad p axis as in Figure 5. **A**: T-state GP*b*. **B**: R-state GP*a*. In the T state (A), there are polar interactions between Asn 270 and Asn 274′ and nonpolar interactions between Val 266 and Leu 267′. In the R state (B), Arg 269 H-bonds to Gln 273′ and Asn 270 to Asn 270′.

sociation of contact 2 (the association of the glycogen storage domain with the $\alpha 25/\alpha 26$ loop) produces the larger change in solvent-accessible surface area, accounting for almost 50% of the total solvent-accessible surface area changed on tetramer formation. The association of tower helices across the r axis causes a change in solvent-accessible surface area of 360 Å^2 per subunit.

Conformational changes

The conserved core

The conformational differences between T-state GP*b* and R-state GP*a* that give rise to changes in the enzyme's surface and may account for the association of dimers to tetramers in the R state have been analyzed by superimposing equivalent subunits. A strategy was developed to identify a conserved core of residues whose positions do not shift and to distinguish these from regions with more substantial conformational changes. A least-squares superimposition was performed to define the set of Cα-atoms that deviate between the two structures by less than an overall r.m.s. of 0.5 Å. This was achieved by performing a global superimposition over residues 10–837 for T and R states that gave an overall r.m.s. difference of 3.7 Å. This reduced to 1.3 Å if residues 10–22 were excluded. The atom pair that deviated most between the two structures was identified and excluded from the set of atoms, a new superimposition was performed, and the r.m.s. deviation redetermined. This filtering process was continued until a subset of atoms representing a structurally conserved core was established. The conserved core comprises 536 Cα-atoms out of a total of 828 (65%) that superimpose to within an overall r.m.s. difference of 0.5 Å. Using this procedure to superimpose structures, a larger number of Cα-atoms superimpose more closely than occurs when a global superimposition is performed designed to minimize the overall r.m.s. deviation. Ta-

Table 3. *Changes in solvent accessibility per subunit on formation of R-state tetramers*

q-axis contacts		r-axis contacts	
Residue number	Area change (Å^2)	Residue number	Area change (Å^2)
Contact1		Arg 205	50
Arg 724	25	Gln 264	62
Asp 722	21	His 390	35
Gln 723	30	Leu 267	60
729	45	271	31
Gly 725	35	Phe 257	48
Contact 2		Thr 394	21
Ala 435	62	Tyr 262	53
Arg 426	87		
770	27		
Asp 423	9		
756	27		
Asn 727	60		
Glu 433	25		
Gln 754	49		
Gly 434	43		
His 767	31		
768	38		
Leu 757	8		
Lys 753	18		
Met 618	5		
Pro 755	25		
Trp 174	33		
Contact 3			
Tyr 262	42		
Ile 263	37		
Total	782	Total	360

Table 4. *Conserved residues between T-state GPb and R-state GPa*

1. The 536 Cα-atoms of a structurally conserved core, which superimpose to within an overall r.m.s. deviation of 0.5 Å between T-state GP*b* and R-state GP*a*.

   52–53, 55–63, 66–105, 108, 110, 111, 119–129, 134–164, 166–184, 187–207, 210–211, 213–247, 267–277, 279, 288–311, 325–356, 358–377, 386–387, 389–407, 409–411, 430–434, 437–438, 440–464, 466–513, 515–522, 524–552, 556–557, 560–567, 598–608, 611–612, 638–665, 672–690, 693–694, 696–711, 780–781, 783–808, 810–833

2. The 379 Cα-atoms that deviate in position by less than 0.5 Å between T-state GP*b* and R-state GP*a* after superimposition of the conserved core matrix. These residues are shaded in Figures 1 and 2.

   55–61, 66–74, 78–104, 122–129, 135–143, 145–162, 179–183, 187–197, 200–207, 215–218, 223–246, 295–308, 330–337, 339–355, 367–376, 392–404, 443–461, 478–506, 517–521, 529–546, 548–551, 562–567, 600–608, 644–663, 673–690, 696–711, 785–808, 811–829

ble 4 indicates that 379 Cα-atoms differ in position by less than 0.5 Å between the two structures when a filtered superimposition is applied, compared to 244 when an overall superimposition is performed. A plot of the r.m.s. deviations in Cα-atom coordinates between R-state GP*a* and T-state GP*b* after a superimposition based on the conserved core operation has been given previously (Barford et al., 1991).

Cα-atoms that differ in position by more than 0.5 Å between the two structures (defined as the core atoms) are depicted by shading in Figures 1 and 2. Within the N-terminal domain, all elements of the central β-sheet form part of the structurally conserved core together with those structural elements most closely associated with it, namely the α2, α3, α6, and α9 helices and the majority of the β8/β9 loop. In the C-terminal domain, the core consists of the β-strands of the dinucleotide-binding fold β19, β20, β22, β23, β24 (except β21), and the α-helices α20, α21, α22 (i.e., structural unit 3 and most of structural units 1 and 5). Two hundred eighteen Cα-atoms of the N-terminal domain and 161 Cα-atoms of the C-terminal domain are present in the core, hence the core encompasses both domains. Regions of the structure where Cα-atoms differ in position by more than 0.5 Å between the two states occur in the subdomains that are peripheral to the main core of the molecule, for instance the cap′/α2 subdomain, the tower helix, the glycogen storage subdomain, and the C-terminal subdomain, together with the 280s and 380s loops located at the catalytic site.

The question of whether relative domain motions occur has been examined (Table 5). For structures superimposed onto the common core, the r.m.s. deviation between Cα-atoms of the N-terminal domain is 0.51 Å, and between Cα-atoms of the C-terminal domain it is 0.47 Å. The transformation required to optimize the fit between two equivalent N-terminal domains involves a rotation of 0.5° to produce a marginally improved r.m.s. deviation of 0.49 Å. Fitting the C-terminal domain produces an r.m.s. deviation of 0.39 Å after a 0.9° rotation. On applying the operation to fit the N-terminal domain to both domains, the r.m.s. deviation between equivalent Cα-atoms of the C-terminal domain rises from 0.39 Å to 0.58 Å and requires a 1.4° rotation to fit the C-terminal domain to an r.m.s. of 0.39 Å (Table 5). The mean positional difference between equivalent Cα-atoms of the N-terminal domain of structures superimposed onto the conserved core and for structures superimposed onto the N-terminal domain is 0.15 Å. The equivalent figure for the C-terminal domain is 0.26 Å. Thus, although a small relative domain motion is suggested by this analysis, the magnitude of the movement is close to the positional accuracy (approximately 0.2–0.3 Å) of the atomic coordinates, and definitive proof for domain motions cannot be established. The majority of interdomain interactions,

Table 5. *Superimposition of domains and subdomains*

Structural element	r.m.s. deviation: no superimposition	r.m.s. deviation: superimposition	Transformation	
			Rotation	Translation
1. Superimposition of conserved CORE Cα atoms from both domains. Overall r.m.s. deviation = 0.50 Å.				
N-terminal domain (CORE atoms)	0.51 Å	0.49 Å	0.5°	0.5 Å
C-terminal domain (CORE atoms)	0.47 Å	0.39 Å	0.9°	0.10 Å
2. Superimposition of conserved CORE Cα atoms of the N-terminal domain. Overall r.m.s. deviation = 0.49 Å.				
C-terminal domain (CORE atoms)	0.58 Å	0.39 Å	1.4°	0.15 Å
3. Superimposition of conserved CORE Cα atoms of the C-terminal domain. Overall r.m.s. deviation = 0.39 Å.				
N-terminal domain	0.69 Å	0.49 Å	1.4°	0.15 Å
4. Superimposition of conserved CORE Cα atoms from both domains.				
a. cap′/α2 subdomain				
cap/α2 (23–58)	1.20 Å	0.36 Å	3.8°	0.27 Å
α4/α5 (104–124)				
b. Glycogen storage subdomain				
α11–α14 (388–448)	1.06 Å	0.40 Å	2.9°	0.28 Å
α15a/α15b (456–475)				
c. C-terminal subdomain				
α18 (568–593)	1.61 Å	0.43 Å	3.9°	−0.2 Å
α19/β21 (608–645)				
α23–α27 (711–785)				

produced by residues of the conserved core, are common between T-state GP*b* and R-state GP*a*, consistent with the notion that there is little relative movement between the domains.

N-terminal domain conformational changes

Previous analysis (Barford et al., 1991) has shown that the regions of the N-terminal domain that show the greatest changes (shifts in Cα atoms >1.2 Å) on the T-to-R transition are: the N-terminal tail residues (10–23), the α1 helix, the cap (residues 39–45), the start of the α2 helix (residues 46–51), the α4 helix (residues 112–118), the catalytic site residues 130–133, the tower helix and 280s loop (residues 260–286), residues 380–382, the glycogen storage subdomain (residues 415–440), and the disordered regions residues 252–256 and 313–324 (Figs. 1, 2). Here we describe the transitions of the N-terminal subdomains. The movements of the tower helices have already been described (Barford & Johnson, 1989; Barford et al., 1991), and those for the concerted motion of the 280s and 380s loops are given later. A description of the changes in the disordered regions is not given because of the uncertainty in the positions of these residues that have high temperature factors and poor electron density.

The cap/α2 subdomain, which forms a major part of the allosteric and Ser-P binding sites, consists of the α1 helix, cap, start of α2 (these units comprise residues 23–58) and the α4 helix, α4–α5 loop, and start of α5 (residues 105–131) . The distance geometry plot (not shown) indicates that all interatomic distances between the Cα-atoms of the subdomain are less than 35 Å and that most interatomic distances between the subdomain and the remainder of the subunit are greater than 35 Å. This indicates that residues of the subdomain are closely associated among themselves and make few interactions with the rest of the subunit (Fig. 1). When T-state GP*b* and R-state GP*a* structures are superimposed with the conserved core matrix, the r.m.s. deviation between Cα-atoms of this subdomain is 1.3 Å. After a rigid body rotation of 3.8° and translation of 0.3 Å, Cα-atoms superimpose to 0.36 Å (Table 5). The rotation occurs about an axis, oriented parallel to the molecular p-dyad axis, located at a point close to the N-termini of α1 and α4 and between His 62 and Gly 65 of α2. A structural discontinuity occurs at this site in the α2 helix where in T-state GP*b*, the helix bends by 30° and is unwound (Barford et al., 1991). Rotation of the subdomain, linked to localized side-chain conformational changes, restores the helix conformation. Figure 9A illustrates the geometric relationship of the cap/α2 subdomain of R-state GP*a* and T-state GP*b* when the conserved cores of the subunits are superimposed. Figure 9B shows the relationship

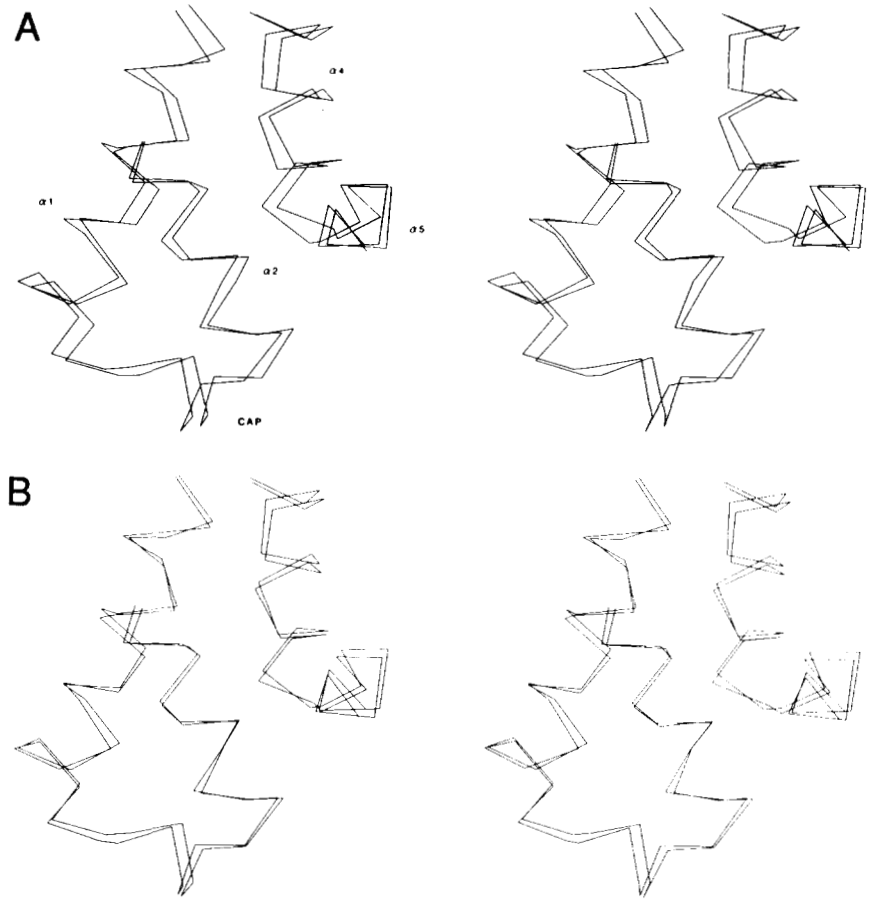

Fig. 9. Stereo views of the cap/α2 subdomain of T-state GP*b* and R-state GP*a*. The view is coincident with the molecular p-dyad axis. **A**: Showing differences in position when subunits are superimposed onto the common core. **B**: After least-squares superimposition of the subdomain.

after a least-squares superimposition of Cα-atoms of the subdomain.

The glycogen storage subdomain (α11, α12, α13, β15, β16, and α14 [residues 387–448] and α15a and α15b [residues 456–475]) also exhibits changes that can be characterized by a rigid body rotation (Table 5). The r.m.s. deviation of Cα-atom coordinates of this subdomain between the two structures superimposed with the conserved core matrix is 1.1 Å. Rigid body rotation of 2.9° about an axis situated close to the midpoint of α14, oriented approximately parallel to the molecular p axis, reduces this difference to 0.4 Å (Fig. 10). Although the glycogen storage subdomain does not participate in the dimer interface, it is affected by changes at the catalytic site and forms part of the tetramer interface.

C-terminal domain conformational changes

The majority of the C-terminal domain forms part of the structurally conserved core, consisting of units 1, 3, and 5 together with the β19 and β20 strands of unit 2. Only α18 and α19 of unit 2 and the α-helices of unit 4 (residues 568–593, 608–645, 711–785, termed the C-terminal subdomain) and the C-terminal residues 838–842 undergo a concerted conformational change and exist outside of the conserved core (Figs. 1, 2b). The r.m.s. deviation between equivalent Cα-atoms of the C-terminal subdomain when T-state GP*b* and R-state GP*a* structures are superimposed with the conserved core matrix is 1.6 Å. Rigid body rotation of 4° about an axis located close to the start of α18 and α19 and oriented parallel to the molecular p axis reduces this difference to 0.49 Å. Figure 11A illustrates the geometric relationship of the α-helices of this subdomain when subunits of R-state GP*a* and T-state GP*b* are superimposed using the conserved core matrix and Figure 11B after least-squares superimposition of Cα-atoms of the subdomain (Table 5). A hydrophobic cluster is formed by the association of α18, α19, α23–α27, and β21. In contrast, a relatively small number of interactions are formed between α18, α19, and β21, and the dinucleotide-binding fold, and no interactions are formed between α23–α27 and other residues of the C-terminal domain. There are no specific side-

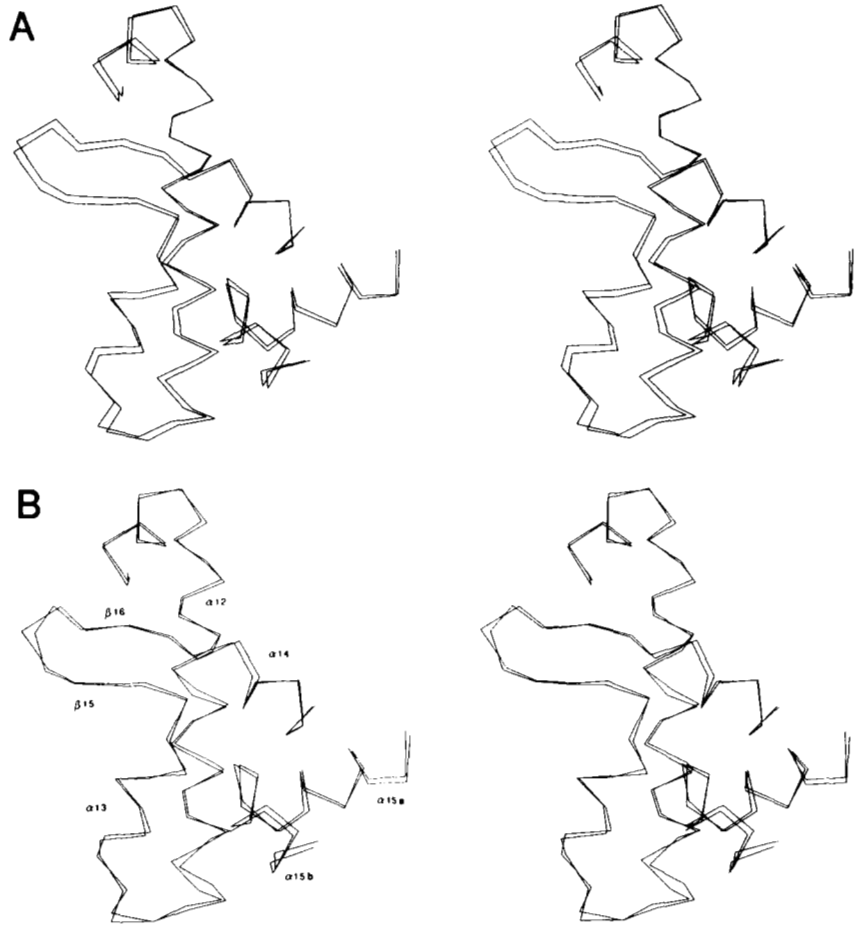

Fig. 10. Stereo views of the glycogen storage subdomain of T-state GP*b* and R-state GP*a*. The structure has been rotated by 45° about a vertical axis with respect to the orientation in Figure 1 and is approximately down the p axis. **A**: Showing differences in position when subunits are superimposed onto the common core. **B**: After least-squares superimposition of the subdomain.

chain–side-chain interactions between α19 or β21 and other elements of the C-terminal domain. An H-bond between Asn 579 of α18 and Gln 566 of β19 is preserved between the two states as a result of side-chain rotation of Gln 566. Thus, the motion of the C-terminal subdomain relative to the C-terminal domain can be achieved as a rigid body motion without changes in side-chain packing, and only in a few instances are side-chain readjustments observed. Motion of the C-terminal subdomain is of a different character to the helix shear motion described for the relative motion of α-helices in, for example, citrate synthase, where contacts between neighboring helices were preserved by adjustment in side-chain conformations (Lesk & Chothia, 1984). The motion of the C-terminal subdomain results in Cα-atoms at the start of the α27 helix differing in position by more than 0.5 Å between the two structures, whereas Cα-atoms of the end of α27 differ by less than 0.5 Å (Fig. 2B). However, this motion is a rigid body motion in which there is no deformation of α27, and the Cα-atoms of the isolated α27 helix from the two states superimpose to within 0.25 Å.

Thus, for both the N-terminal and C-terminal subdomains, the changes can be treated as a rigid body motion characterized by a rotation about an axis parallel to the p (dimer) axis. After the suitable transformations the Cα-atoms of the residues in these domains superimpose to within the limits defined for the conserved core residues.

Interdomain interactions

The majority of the interdomain contacts are preserved between the R and T states, with a relatively small number being unique to a particular state. The location of interdomain contacts in the molecule (H-bonds, salt bridges, and van der Waals contacts) are indicated in Figure 2. Those interactions common to both states are indicated by O, whereas those unique to R and T are indicated as R and T, respectively. Specifically, 44 H-bonds and ionic bridges are identical in both the R and T states with 8 unique to T and 4 unique to R. A total of 87 van der Waals contacts are common between the two

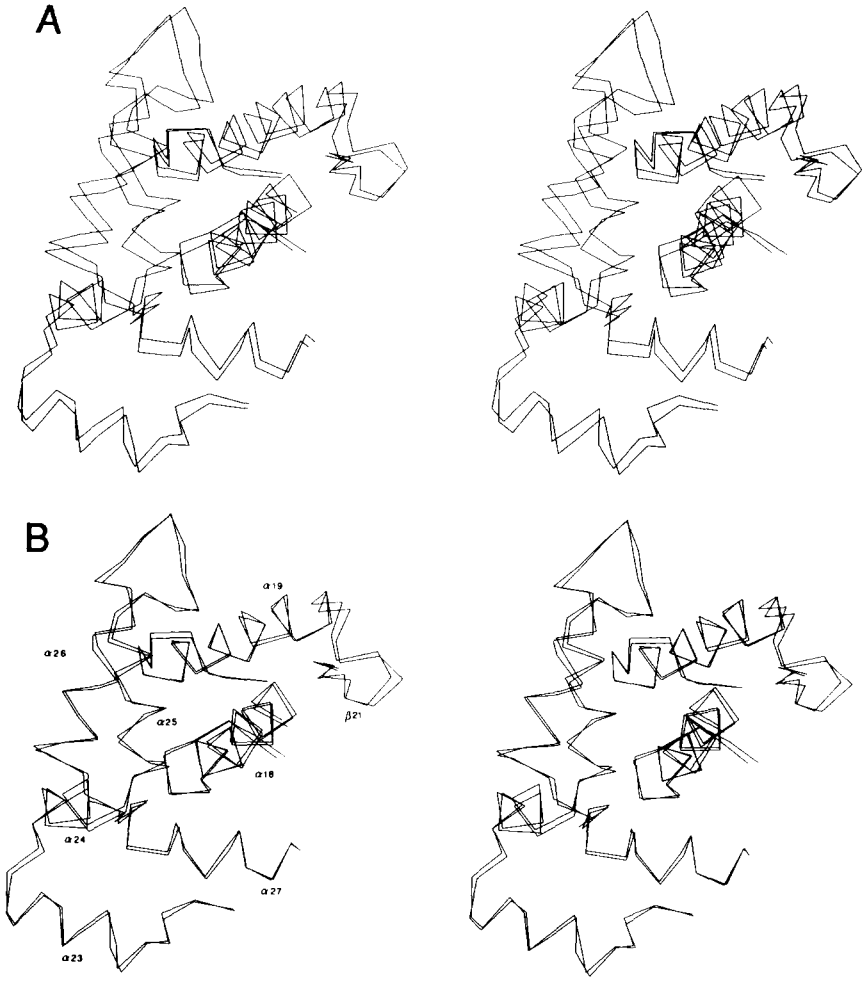

Fig. 11. Stereo views of the C-terminal subdomain of T-state GP*b* and R-state GP*a*. **A**: Showing differences in position when subunits are superimposed onto the common core. **B**: After least-squares superimposition of the subdomain.

states with 6 unique to T and 2 unique to R. Interdomain contacts that differ between R-state GP*a* and T-state GP*b* are listed in Table 6. Almost all interdomain contacts common to both structures occur within the conserved core of the protein. The few exceptions described below are due to compensatory conformational changes in the N- and C-terminal domains. As would be expected, all contacts unique to either state occur in the unconserved regions. The conservation of interdomain contacts is reflected in similar values for solvent-accessible area buried on formation of the domain interface for T and R states (6,564 Å^2 and 5,594 Å^2, respectively). The larger surface area buried at the T-state domain interface, 970 Å^2, is largely accounted for by the opening of the catalytic site tunnel in the R state as a result of motion of the 280s and 380s loops and the C-terminal subdomain.

The additional number of interdomain contacts occurring in the T-state of GP*b* compared to the R state of GP*a* are located at the catalytic site. The rupture of these interactions on conversion from T to R plays a role in increasing the affinity of the R state for phosphate. In T-state GP*b*, the side-chain of Arg 569 forms H-bonds to the side-chain and main-chain carbonyl of Asn 133, the main-chain carbonyl of Pro 281, and an additional intradomain contact to main-chain carbonyl of Lys 608. Residues of the 280s loop that are ordered in the T state also participate in interdomain contacts; for example, the side-chain of Asp 283 forms a salt bridge to His 571, and residues Pro 281, Asn 282, and Asp 284 form van der Waals contacts to Ala 610 and Pro 611, His 571 and Tyr 573 (Table 6).

On conversion to the R state, the tilt of the tower helices shifts Tyr 262′ and perturbs the conformation of Asn 133 and Pro 281. Motion of Asn 133 and Pro 281 disrupts their interaction to Arg 569, the side chain of which shifts by 7 Å. A concerted disordering of the 280s loop occurs, which removes Asp 283 from the vicinity of the catalytic site and the previous position of Asp 283 is occupied by the side chain of Arg 569. The interchange of an acidic by a basic residue creates a high-affinity

Table 6. *Interdomain contacts*

			a		b		
A. H-bonds and salt bridges between R-state GP*a* and T-state GP*b* < 0.35 Å							
1. Interactions unique to T-state GP*b*							
Asn 133 O	Arg 569 NH1	–	–	–	–	β3/α6-β19
Asn 133 OD1	Arg 569 NH1	–	–	–	–	
Asn 167 OD1	Asn 647 ND2	*	*	–	*	β5-β21/α20
Asn 168 OE1	Asn 647 N	*	*	–	*	β5-β21/α20
Pro 281 O	Arg 569 NH2	–	–	–	–	280s-β19
Asp 283 O	His 571 NE2	–	–	–	–	280s β19/α18
Asp 283 OD2	His 571 NE2	–	–	–	–	280s β19/α18
Glu 382 OE2	Arg 770 NH1	–	–	–	–	β13/β14 α26/α27
2. Interactions unique to R-state GP*a*							
Asn 167 ND2	Asn 647 OD1	*	*	–	*	β5-β21/α20
Asn 168 NE2	Leu 645 O	*	*	–	*	β5-β21
Lys 169 NZ	Glu 646 OE1	*	*	–	*	β5-β21/α20
Tyr 233 OH	Glu 509 OE1	*	*	*	–	β10/β11-3_{10}
B. Interdomain van der Waals contacts >4.0 Å							
1. Interactions unique to T-state GP*b*							
Asn 133	Arg 569	–	–	–	–	β3/α6-β19
Ile 165	Lys 608	–	*	–	*	β5-β20
Lys 169	Glu 646	*	*	–	*	β5-β21/α20
Pro 281	Arg 569	–	–	–	–	280s-β19
Pro 281	Pro 611	–	*	–	–	280s-β20/α20
Glu 382	Arg 770	–	–	–	–	β14-α26/α27
2. Interactions unique to R-state GP*a*							
Val 379	Thr 671	–	–	–	–	β14-β22/α21
Val 379	Ala 673	–	–	–	–	

[a] * indicates that residue occurs within the structurally conserved core that superimposes to an overall r.m.s. deviation of 0.5 Å; – indicates that residue does not occur within the conserved core. Contacts are listed if they occur in two or more subunits.

[b] * indicates that Cα-atom coordinates differ by less than 0.5 Å between T-state GP*b* and R-state GP*a*; – indicates that Cα-atom coordinates differ by more than 0.5 Å between T-state GP*b* and R-state GP*a*. Contacts are listed if they occur in two or more subunits.

phosphate-binding site adjacent to the phosphate of pyridoxal 5′-phosphate. Disordering of the 280s loop allows access to the catalytic site (Fig. 12; Kinemage 8).

In the T state, the 280s loop packs against a loop formed by residues 377–384 (the 380s loop). On transition to the R state, disordering of the 280s loop is correlated with a conformational change of the 380s loop. Displacement of Glu 382 by 4.5 Å and subsequent rupture of the salt bridge between Glu 382 and Arg 770 of the C-terminal subdomain occurs (Fig. 12).

The interdomain interactions produced between the β5/β6 sheet of the N-terminal domain and the α19 helix and β21 strand of the C-terminal domain are largely conserved, although these regions differ by more than 0.5 Å between the two states. The conformational change of one region is compensated for by a conformational change in the other, preserving interdomain contacts. Residues Asn 167 and Lys 169 of the β5 strand form different interdomain contacts between the two states. In T-state GP*b*, OD1 of Asn 167 forms an H-bond to ND2 of Asn 647, whereas in R-state GP*a*, ND2 of Asn 167 forms an H-bond to OD1 of Asn 647 (Fig. 13). The conformation of the side chain of Lys 169 differs between R-state GP*a* and T-state GP*b* and in the R state forms a salt bridge to the side chain of Glu 646 (Fig. 13).

Discussion

Transmission of conformational signals

The key event in the activation of glycogen phosphorylase is the increase in enzymic activity following conformational changes at the catalytic site, which result in enhanced affinity for substrates; phosphate, Glc-1-P, and oligosaccharides. Binding of AMP to the allosteric site or phosphorylation of Ser 14 of dimeric GP*b* favors a tertiary conformational change in the region of the molecule associated with the cap′/α2 interface and an associated change in quaternary structure. The change in quaternary conformation is linked to a change in the packing geometry of the symmetry-related tower helices on the far side of the molecule from the cap′/α2 interface. Tilting of the tower helices relative to the remainder of the molecule transmits a signal from the subunit interface to the catalytic site (that includes displacement of the 280s loop) and provides a route for transmission of conformational

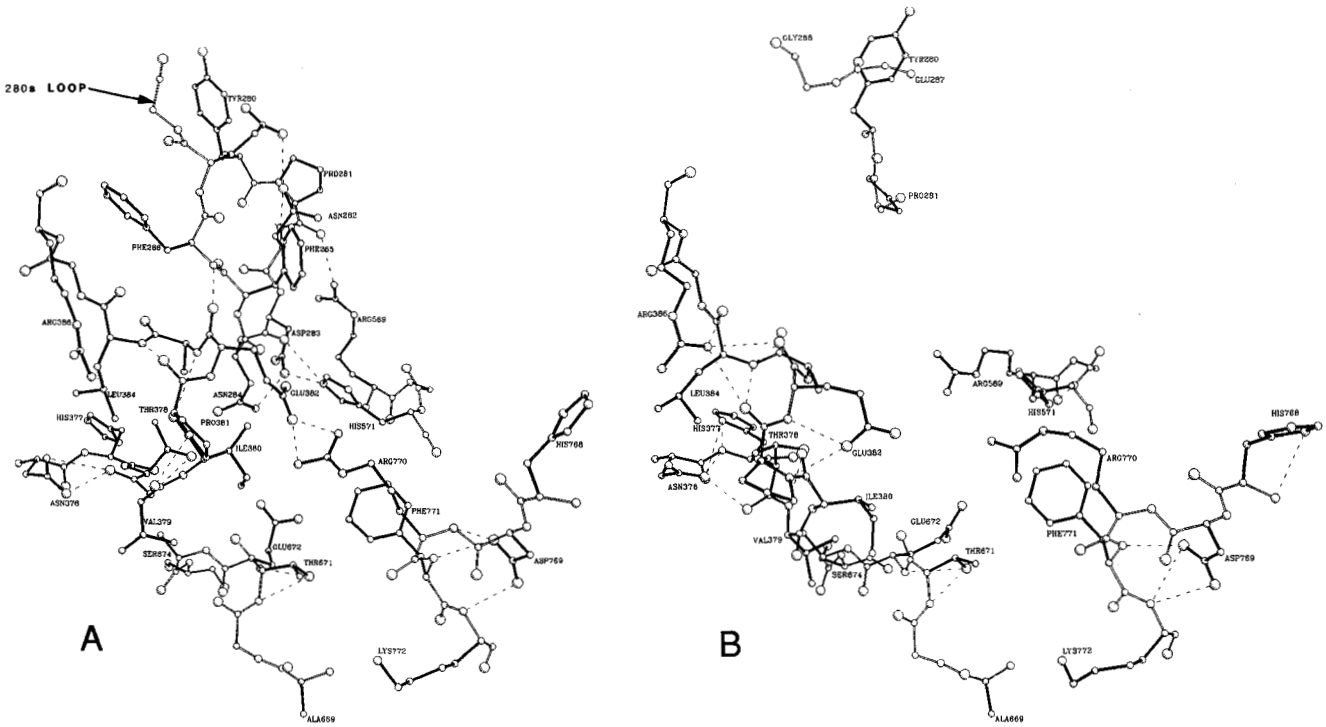

Fig. 12. Details of the conformational changes occurring at the catalytic site on transition from T-state GP*b* (**A**) to R-state GP*a* (**B**). Disordering of the 280s loop (residues 282–286) and shifts in the 380s loop (residues 377–384) occurs on conversion from T to R. The salt bridge between Glu 382 and Arg 770 in T-state GP*b* is broken in R-state GP*a*.

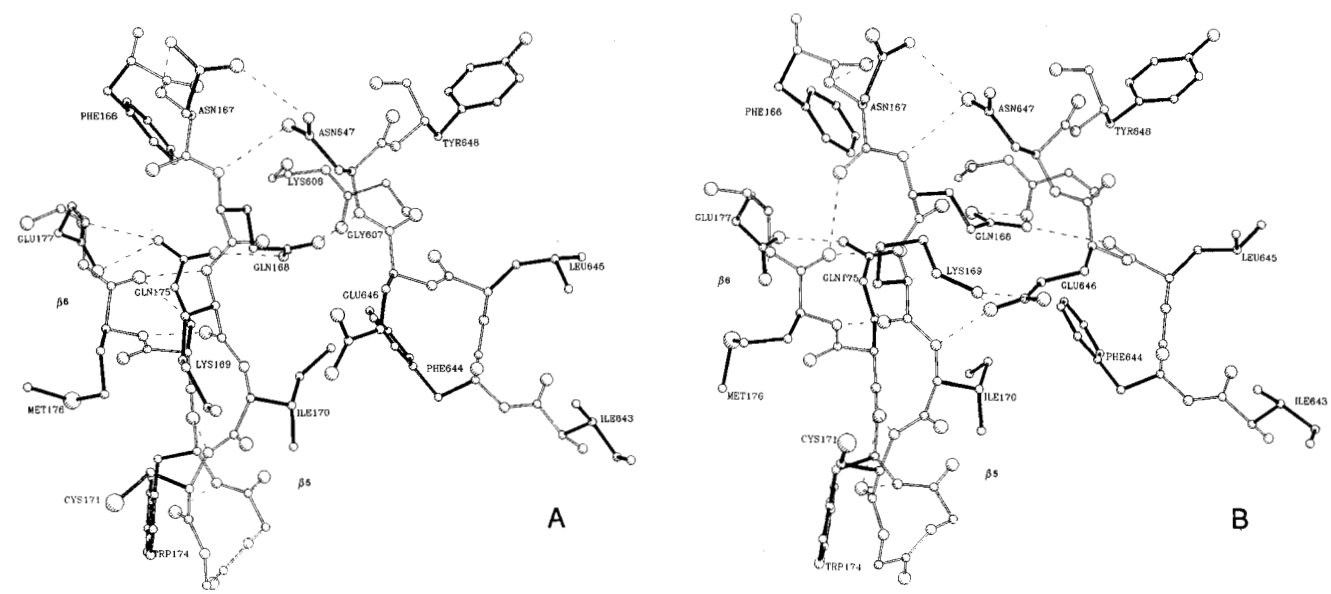

Fig. 13. Interactions between β5/β6 of the N-terminal domain to β21 of the C-terminal domain in T-state GP*b* (**A**) and R-state GP*a* (**B**). There is an interaction formed between Lys 169 and Glu 646 in GP*a* not formed in GP*b*.

signals to other regions of the molecule. In solution, activation (in the absence of glycogen) and tetramerization are intimately linked so that it is plausible to assume that the changes in the surface arising from the T-to-R transition are correlated with the formation of new surface properties that lead to tetramer formation. The catalytic site structure is affected by ligation of AMP at the allosteric site or Ser 14 phosphorylation occurring at the p

(dimer) interface of the molecule. The conformational changes at this interface promote the formation of the new q and r interfaces. The present analysis has shown that those regions involved in the tetramer interface are located on subdomains on the enzyme surface, the glycogen storage subdomain, the C-terminal subdomain, and the tower helix.

Comparison between the T- and R-state molecules shows that each of these subdomains undergoes a rigid body motion relative to the main body of the subunit that is characterized by a rotation about an axis parallel to the twofold axis of the dimer. The movements of the C-terminal subdomain and of the glycogen storage subdomain are of opposite sign. (These relative movements are also apparent in Fig. 1c,d in Barford et al. [1991].) The motion of subdomains leads to a widening of the catalytic site tunnel with the result that the distance between Asp 423 of the glycogen storage subdomain and Gln 723 of the C-terminal subdomain increases from 23 Å to 27 Å. Some rationalization for these movements can be provided by the changes at the catalytic site. Motion of the 280s loop and the correlated shifts of the 380s loop (residues 377–384) on conversion to the R state leads to disruption of certain interdomain interactions. For example, on the T-to-R transition H-bonds are broken between the side chain of Arg 569 and Asn 133 and Pro 281, a salt bridge between His 571 and Asp 283 is broken, and a new H-bond is formed between His 571 and the side chain of Tyr 613. Shifts in the 280s loop perturb the 380s loop (Fig. 12), and the salt bridge between Glu 382 (on the loop between β13 and β14) and Arg 770 (on the loop between α26 and α27 of the C-terminal subdomain) is broken. This disrupts the major link between the glycogen storage subdomain and the C-terminal subdomain. The weakening of the interactions that govern the association of the C-terminal subdomain to the body of the subunit provides a rationalization for the reorganization of the semiautonomous unit on the T-to-R transition. Rationalization for the shifts of the glycogen storage subdomain is less easy, but we note the connection between the 380s loop and the start of the α15a helix and the connection through the antiparallel β-sheet β14, β15, β16 to residues Glu 433 and Lys 437 that make key interactions to oligosaccharides bound at the glycogen storage site. Perturbation of these interactions could promote the shifts of the subdomain.

The association of dimers to tetramers partially blocks access to the catalytic site and provides an explanation for the lower activity of the R-state tetramers (Metzger et al., 1967; Huang & Graves, 1970). The involvement of the glycogen storage subdomain explains the ability of glycogen to dissociate tetramers. Model-building studies suggest that short-chain oligosaccharides may be accommodated at this site, and this has been supported by the observation that maltose binds to the glycogen storage site in tetrameric R-state GP*b* in the crystal (Hu, 1991). The disaccharide occupies the highest affinity subsites, S4 and S5 (as defined in Johnson et al., 1988, 1990). The interactions between oligosaccharide bound to subsites S4 and S5 and Arg 426 and Glu 433 are formed in the R state despite the proximity of these residues to the tetramer interface. Crystallographic binding studies with longer oligosaccharides are in progress. However, the model suggests that longer chain oligosaccharides or glycogen would have difficulty in binding to the glycogen storage site in the tetramer and that the association of glycogen with this site in the dimer would impede formation of tetramers.

Structural properties of the subunit interfaces

On the T-to-R conversion, the correlated movements of the subdomains lead to a new aggregation surface. As a result of these movements and the global quaternary structure change in which one subunit rotates 10° with respect to the other, there is a change in the shape of the surface of the dimeric enzyme, from a concave to a more flat surface in the face about the q axis that forms the tetramer interface (see, for example, Fig. 1e,f in Barford et al. [1991]). Formation of the specific interactions at the tetramer interface requires both these tertiary and quaternary conformational changes. Model-building studies with a hybrid tetramer formed from the R-state quaternary structure and T-state tertiary structure indicates that, across the q axis, residues at both contacts pack to within 1 Å. This close packing is alleviated, and specific interactions are formed following tertiary conformational changes involving concerted motion of subdomains, main-chain atoms at both contacts, and side-chain motions at contact 2. Within each subdomain relatively few conformational changes occur.

The tetramer interface comprises only 3% of the total accessible surface area of the isolated subunit, and the surface area buried is 1,142 Å^2. The interface especially across the q axis is predominantly polar including four H-bonds and two salt bridges. The van der Waals interactions are mostly through the nonpolar components of the polar side chains (Table 2). Tyr 262 is the major exception, and this residue forms van der Waals interactions to Ile 263″ about the q axis and to Leu 267‴ and Leu 271‴ about the r axis. Each of these contacts with Tyr 262 involves residues from the tower helices. The polar q interface is established even in the presence of 1 M ammonium sulfate (the salt used for crystallization). However, the interface can be disrupted by NaCl at similar ionic strength, as in 3 M NaCl GP*a* dissociates to dimers (Wang & Graves, 1963, 1964).

The difference in the chemical nature of the solvent-accessible areas at the different interfaces is remarkable. The surface of the isolated subunit of phosphorylase is approximately 54% nonpolar. (The definitions of the nonpolar and polar surfaces are given in the Methods sec-

tion.) This value is similar to the value, 57% (3), found by Janin et al. (1988) in a survey of 34 monomeric and 18 oligomeric proteins for the nonpolar component of the surfaces of isolated subunits (where the number in parentheses is the standard deviation). In phosphorylase, the p interface is approximately 65% nonpolar for T-state GP*b* and a similar value is obtained for R-state GP*a*, where the nature of the interactions and the accessible area buried are similar despite the substantial conformational changes (Barford & Johnson, 1989). Janin et al., in their survey of oligomeric protein interfaces, found that these were generally more nonpolar than the surface of the subunits and calculated an average value of 65% (4) for the nonpolar component of the subunit-interface areas. Thus, the nonpolar character of the p interface of phosphorylase is typical of other oligomeric proteins. The q interface is different. It is only 52% nonpolar and is more typical of the surface of the subunit as a whole. The small r interface, which contributes only 11% to the change in solvent-accessible area on tetramerization, is nonpolar (70% nonpolar) as a result of the Tyr/Leu/Ile associations at this interface.

The q interface also differs from other oligomeric interfaces in the number of H-bonds. Janin et al. (1988) found that the smaller interfaces of oligomeric proteins had few H-bonds and that for interfaces greater than 1,500 Å^2 the average number of H-bonds was about one per 200 Å^2 of interface area. The H-bonds at the q-tetramer interface are more numerous (i.e., six H-bonds in 782 Å^2 corresponding to one per 130 Å^2) than those of an oligomeric protein, whereas those at the p-dimer interface are more typical (one per 190 Å^2). In surveying the characteristics of protein recognition sites formed by protease–inhibitor complexes and antibody–protein antigen complexes, Janin and Chothia (1990) showed that the nature of the surface recognition area in these complexes is similar to the accessible surface of the isolated proteins, and the number of H-bonds formed is typically one per 141 Å^2 (ranging from one per 225 Å^2 to one per 103 Å^2 for 15 examples). Thus, in its chemical character, the q interface is more akin to the recognition contact surface at protein–protein complexes than a typical interface of an oligomeric protein. The interface reflects complementarity of shape and specific polar interactions rather than dominant nonpolar interactions. In the presence of glycogen or on dilution, tetramers of glycogen phosphorylase dissociate to form functional dimers and the dimeric species are stable entities. Similarly, the components of protease–inhibitor complexes and antibody–protein antigen complexes are stable in isolation.

The standard enthalpy and entropy changes for dissociation (by dilution) of GP*a* tetramers to dimers obtained from activity measurements at pH 6.8 and a temperature range of 20–35 °C gave values of 60 kcal/mol and 170 eu, with a standard free energy change of 10 kcal/mol at 20 °C (Huang & Graves, 1970). The authors commented on the enthalpic nature of the energy of association. Similar values were obtained from light-scattering experiments. Attempts to relate energy values calculated from the observed interactions to the experimentally derived values encounter several difficulties. The energy observed on formation of the tetramer interface has favorable contributions from the H-bonds, van der Waals interactions, and the hydrophobic effect derived from burying some nonpolar groups and unfavorable components from the increased order in the system, loss of rotational and translational entropy, disruption of protein–water interactions, and possibly energy loss due to promotion of conformational changes at the interface. Fersht et al. (1985) have shown that H-bonds contribute between 0.8 and 1.8 kcal/mol for polar groups and between 3 and 6 kcal/mol for charged groups. The tetramer interface has four polar H-bonds and two H-bonds between charged groups per subunit. The charged interactions involve the same residues, and an estimate of 3 kcal/mol is made for this interaction. Together the H-bonds and ionic interactions could contribute between 6 and 10 kcal/mol to the overall free energy change per subunit. Estimates of van der Waals interactions are more difficult to make. They depend not only upon the distance between nonbonded atoms but also the nature of the interacting groups, and no attempt is made here to estimate their contribution. Chothia (1974) has shown that the hydrophobic contribution may be approximated by a free energy gain of 25 kcal/mol per 1 Å^2 of accessible surface area buried. The energy terms, which are largely entropic, were taken from the free energy changes observed in the transfer of amino acids from water to organic solvents. A similar entropic change might be anticipated for burying residues at the tetramer interface, although the interface is mostly polar. The observed change in accessible surface area is 1,142 Å^2 per subunit, and this corresponds to an energy change of 29 kcal/mol per subunit. A number of authors (referred to in Janin & Chothia, 1990) have estimated that the translational and rotational entropies lost on formation of dimers is about 15 kcal/mol. Thus, the total calculated free energy change from polar contacts, change in surface-accessible area, and loss of entropy is between 20 and 24 kcal/mol per subunit. This is greater than the experimental value (10 kcal/mol per tetramer [Huang & Graves, 1970; Huang, pers. comm.]) and suggests that, in addition to the uncertainties associated with the calculations (that neglect van der Waals interactions), the loss of solvation energy and conformational changes may be important. The occurrence of localized conformational changes involving side-chain rotations on formation of contact 2 at the q-tetramer interface may represent some of these conformational changes.

The change in tertiary structure accompanying quaternary conformational changes observed in oligomeric allosteric proteins is closely correlated with modifications of the energy and nature of intersubunit interactions (re-

viewed by Perutz, 1989; Johnson & Barford, 1990). To a lesser extent formation of protein-inhibitor and antibody-protein antigen complexes also produces small but significant conformational changes (Janin & Chothia, 1990). These include amino acid side-chain rotations on formation of protein-inhibitor complexes, side-chain rotations in the protein antigen, and rearrangements of the V_H and V_L domains of the antibody on formation of antibody-protein antigen complexes (Bhat et al., 1990; Davies et al., 1990). Although the structure of the R-state GP*a* in the dimer oligomerization state is not known, it is likely that it is similar to that of the associated dimer in the tetramer. The major conformational changes observed on activation can be linked to the changes at the catalytic site and the accompanying changes at the more substantial p interface that allows communication to the allosteric and Ser-P sites. The conformational changes required to form the tetramer interface (i.e., movement of the C-terminal subdomains and the glycogen domain) are closely correlated with these changes. In view of the small contact surface at the tetramer interface it seems unlikely that association would promote a major change in the same way as lattice contacts in a crystal do not distort a protein structure, although the lattice contacts may favor some local conformational changes in side chains.

Domain interactions

The subunit of phosphorylase may be divided into the N-terminal and C-terminal domains. The present analysis shows that no significant relative global domain movements occur on transition from the T-state to the R-state structures but that the structural changes can be accounted for by movements of surface subdomains. This is suggested from three observations. Firstly, a conserved core of 65% of the residues from the whole subunit superimposes to within an overall r.m.s. deviation of 0.5 Å between the two states. The conserved core comprises residues from both domains. Secondly, the differences (of the order of 0.2 Å) in coordinates after the transformations required to optimize the fit of conserved cores of individual N- and C-terminal domains (after superimposing the conserved core of the subunit) are similar in magnitude to the positional accuracy of the atomic coordinates. Thirdly, nearly 90% of interdomain H-bonds and 95% of interdomain van der Waals interactions are conserved between the T and R states. Almost all of the changes at the interdomain interface can be attributed to substantial changes in individual residues (e.g., Arg 569) and the displacement of the 280s loop on the T-to-R transition.

However, a slightly different interpretation of the domain movements has come from other crystallographic work. In a binding study of oligosaccharide and phosphate to T-state GP*a* in the crystal, substantial conformational changes were noted that we can now recognize as the initial stages of the T-to-R transition (Goldsmith et al., 1989). The crystals had been grown in the presence of the inhibitor glucose and the glucose removed by soaking. As is common with allosteric proteins, the lattice forces of the T-state crystals prevented the full manifestation of the allosteric response, and it was remarkable that the enzyme had been able to respond so substantially. The global movements were interpreted as a rotation of the C-terminal domain by about 1° relative to the N-terminal domain, and the significance of this rotation for opening up the catalytic site channel as noted. Because in this study the whole domains were apparently used in the determination of the superimposition matrices, the movements of the individual subdomains could have been obscured in the global superimpositions. In a more recent study, the structure of an R-state tetrameric GP*b* with the modified cofactor pyridoxal pyrophosphate cocrystallized in the presence of AMP and oligosaccharide from polyethylene glycol solutions has been solved (Sprang et al., 1991). The overall structure is similar to the sulfated GP*b* structure (Barford & Johnson, 1989) and contributes new information on the binding of AMP. Sprang et al., however, interpret the shifts that occur between the T and R structures to a rotation of the C-terminal domain by 5° relative to the N-terminal domain. In this work, the domains were defined by their β-sheet cores, a different definition to the conserved core in the present work but one that leads to identification of mostly similar core residues. As in the present work, the opening of the catalytic site channel was noted, and the increase in separation of residues from the C-terminal subdomain to those from the glycogen storage subdomain is also similar to that noted in the present work. The analysis presented here has shown that most of the shifts between the T- and R-state subunit structures can be interpreted by movements of surface subdomains relative to a conserved core, which encompasses both the N-terminal domain and the C-terminal domain (see Kinemage 7). Whether the differences in the interpretation of domain movements are a result of different definitions or genuine structural differences remains to be established.

The conservation of the majority of the interdomain contacts has implications for the cofactor and substrate binding sites. Pyridoxal phosphate 680 is contained within the structurally conserved core and does not undergo conformational change on the T-to-R transition. The major contacts between the cofactor and enzyme include interactions with Tyr 648, Arg 649, Val 650, Ala 653 of the α20 helix, Gly 675, Thr 676 of α21, and Tyr 90 of the α6 helix of the N-terminal domain (Oikonomakos et al., 1987), and there are essentially no changes in these contacts. Helices α6, α20, and α21 all form part of the structurally conserved core (Fig. 2). The cofactor 5′-phosphate forms a salt bridge to Lys 568 of the C-terminal subdomain. Lys 568 does shift, but the motion of the main chain of Lys 568 is compensated for

by a side-chain rotation that maintains the salt bridge to the phosphate of pyridoxal phosphate. Residues participating in the binding of the glucosyl component of the Glc-1-P binding site are largely unchanged on conversion to the R state, and the changes that do occur affect the C-1 atom and phosphate group. Residues important in binding the glucosyl moiety of Glc-1-P are the side chains of His 377, Asn 484, Tyr 573, and Glu 672 and main-chain atoms of Ala 673, Ser 674, and Gly 675, all of which (except Tyr 573) are part of the conserved core of the protein. Asn 284, which in the T state forms an H-bond to the O2 hydroxyl group of glucose but not to Glc-1-P or 2FGlc-1-P (Martin et al., 1990), is displaced in the R state. The phosphate recognition site in the R state is formed from the side chains of Arg 569, Lys 574, the phosphate of pyridoxal 5′-phosphate, and the main-chain N of Gly 135 (Johnson et al., 1990). Motion of the C-terminal subdomain is correlated with the shifts in the main chains of Arg 569 and Lys 574 and with a substantial motion of the side chain of Arg 569 as noted above so that it can contribute to the phosphate recognition site. Residues that are in contact to the phosphate group of Glc-1-P in the T state, namely Gly 134, Gly 135, and Leu 136, are largely conserved. Residues Gly 130, Leu 131, Gly 132, and Asn 133 undergo some shifts, but these do not affect the Glc-1-P binding site. Comparison of Glc-1-P bound to R-state and T-state GP*b* (Martin et al., 1990; Hu, 1991) shows that the conformation of the sugar phosphate is very similar in the two structures, and the major differences reside in the additional contacts to the sugar phosphate group in the R state.

In summary, protein phosphorylation leads to an allosteric conformational change consisting of quaternary and tertiary changes within a functional glycogen phosphorylase dimer. This is accompanied by an association of the dimers to a tetramer. The tetramer interface recognition surface is closely dependent on the conformational changes within the functional dimer. Conversely, it might be expected that protein association requiring the correct juxtaposition of residues within the interface will stabilize the activated conformation of the protein. Allosteric effectors and protein phosphorylation control association/dissociation events by modulating the conformation of the subunit and hence its recognition surface to another protein or subunit.

Methods

The tetrameric R-state GP*a* structure at 2.9 Å resolution refined to an *R*-factor of 0.176 (Barford et al., 1991) has been compared to the structure of dimeric T-state GP*b* determined to 1.9 Å resolution refined to an R-factor of 0.19 (Acharya et al., 1991). The precision of the atomic coordinates has been discussed in previous publications and is estimated to be about 0.2–0.3 Å for the R-state molecule and slightly better than 0.2 Å for the T-state molecule. Protein coordinates were examined on an Evans and Sutherland PS300 on-line to a VAX 6210 computer with the program FRODO (Jones, 1978) modified by J.W. Pflugrath, M. Saper, R.E. Hubbard, and P.R. Evans. Superimposition of protein coordinates was performed by the program SUPERSIEVE (D. Barford, unpubl.) adapted from the least-squares superimposition algorithm of S.J. Remington based on the method of Kabsch (1978). The program provides the facility of defining a subset of atoms that superimpose within a desired r.m.s. deviation. In this study, a core of Cα-atoms that superimpose to within an r.m.s. difference of 0.5 Å was defined. A superimposition of the two structures was performed based on this superimposition matrix, and the Cα-atom pairs that differ in position by less than 0.5 Å were defined. Other least-squares superimpositions were performed using the method of Hendrickson (1979), implemented in the program ASH (D.I. Stuart, unpubl.).

Solvent-accessibility calculations were determined using the algorithm of Lee and Richards (1971) as implemented by T.J. Richmond with a water probe of 1.4 Å. The percentage nonpolar surface area was calculated from the sum of the solvent-accessible areas for all carbon and sulfur atoms, with the exception of the carbonyl carbon atoms of the main chain, divided by the solvent-accessible area for all atoms. This is similar to the method of Janin et al. (1988), except that Janin et al. excluded sulfur atoms and included main-chain carbonyl carbon atoms in their definition of nonpolar groups.

The coordinates of T-state GP*b* and R-state GP*a* have been deposited in the Brookhaven Protein Data Bank and numbered 9GPB and 1GPA, respectively.

Acknowledgments

This work has been supported by the Medical Research Council and the facilities of the Oxford Centre for Molecular Sciences. We also acknowledge the contributions of our colleague S.-H. Hu to the structural studies on phosphorylase *a*.

References

Acharya, K.R., Stuart, D.I., Varvill, K.M., & Johnson, L.N. (1991). *Glycogen Phosphorylase: Description of the Protein Structure.* World Scientific, London, Singapore.

Barford, D., Hu, S.-H., & Johnson, L.N. (1991). Structural mechanism for glycogen phosphorylase control by phosphorylation and AMP. *J. Mol. Biol. 218*, 233–260.

Barford, D. & Johnson, L.N. (1989). The allosteric transition of glycogen phosphorylase. *Nature 340*, 609–614.

Bhat, T.N., Bentley, G.A., Fischmann, T.O., Bonlet, G., & Poljak, R.J. (1990). Small rearrangements in structures of Fv and Fab fragments of antibody D1.3 on antigen binding. *Nature 347*, 483–485.

Black, W.J. & Wang, J.H. (1968). Studies on the allosteric activation of glycogen phosphorylase *b* by nucleotides. *J. Biol. Chem. 243*, 5892–5898.

Buc, H. (1967). On the allosteric interaction between 5′AMP and orthophosphate on phosphorylase b: Quantitative kinetic predictions. *Biochem. Biophys. Res. Commun. 28*, 59–64.

Chothia, C. (1974). Hydrophobic binding and accessible surface area in proteins. *Nature 248*, 338–339.

Davies, D.R., Padlan, E.A., & Sheriff, S. (1990). Antibody-antigen interactions. *Annu. Rev. Biochem. 59*, 439–473.

Davis, C.H., Schlisefield, L.H., Wolf, D.P., Leavitt, C.A., & Krebs, E.G. (1967). Interrelationships among glycogen phosphorylase isozymes. *J. Biol. Chem. 242*, 4824–4833.

Engers, H.D. & Madsen, N.B. (1968). The effects of anions on the activity of phosphorylase b. *Biochem. Biophys. Res. Commun. 97*, 513–519.

Fersht, A.R., Shi, J.P., Knill-Jones, J., Lowe, D.M., Wilkinson, A.J., Blow, D.M., Brick, P., Carter, P., Waye, M.M.Y., & Winter, G. (1985). Hydrogen bonding and biological specificity analysed by protein engineering. *Nature 314*, 235–238.

Goldsmith, E.J., Sprang, S.R., Hamlin, R., Xuong, N.-H., & Fletterick, R.J. (1989). Domain separation in the activation of glycogen phosphorylase *a*. *Science 245*, 528–532.

Graves, D.J. & Wang, J.H. (1972). α-glucan phosphorylases—Chemical and physical basis of catalysis and control. In *The Enzymes*, 3rd Ed., Vol. 7 (Boyer, P.D., Ed.), pp. 435–482. Academic Press, New York.

Helmreich, E. & Cori, C.F. (1964). The role of adenylic acid in the activation of phosphorylase. *Proc. Natl. Acad. Sci. USA 51*, 131–138.

Hendrickson, W.H. (1979). Transformations to optimize the superposition of similar structures. *Acta Crystallogr. Sect. A 35*, 158–173.

Hu, S.-H. (1991). Crystallographic studies on activated glycogen phosphorylase. Ph.D. Thesis, University of Oxford.

Huang, C.Y. & Graves, D.J. (1970). Correlation between subunit interactions and enzymatic activity of glycogen phosphorylase *a*. Method for determining equilibrium constants from initial rate measurements. *Biochemistry 9*, 660–671.

Janin, J. & Chothia, C. (1990). The structure of protein-protein recognition sites. *J. Biol. Chem. 265*, 16027–16030.

Janin, J., Miller, S., & Chothia, C. (1988). Surface, subunit interfaces and interior of oligomeric proteins. *J. Mol. Biol. 204*, 155–164.

Johnson, L.N. (1992). Glycogen phosphorylase: Control by phosphorylation and by allosteric effectors. *FASEB J. 6*, 2274–2337.

Johnson, L.N., Acharya, K.R., Jordan, M.D., & McLaughlin, P.J. (1990). Refined crystal structure of the phosphorylase heptulose-2-phosphate oligosaccharide-AMP complex. *J. Mol. Biol. 211*, 645–661.

Johnson, L.N. & Barford, D. (1990). Glycogen phosphorylase. The structural basis of the allosteric response and comparison with other allosteric proteins. *J. Biol. Chem. 265*, 2409–2412.

Johnson, L.N., Cheetham, C., McLaughlin, P.J., Acharya, K.R., Barford, D., & Phillips, D.C. (1988). Protein-oligosaccharide interactions: Lysozyme, phosphorylase, amylase. *Curr. Top. Microbiol. Immunol. 139*, 81–134.

Johnson, L.N., Hajdu, J., Acharya, K.R., Stuart, D.I., McLaughlin, P.J., Oikonomakos, N.G., & Barford, D. (1989). Glycogen phosphorylase. In *Allosteric Enzymes* (Herve, G., Ed.), pp. 81–127. CRC Press, Boca Raton, Florida.

Jones, A.T. (1978). A graphics model building and refinement system for macromolecules. *J. Appl. Crystallogr. 11*, 268–272.

Kabsch, W. (1978). A discussion of the solution for the best rotation to rotate two sets of vectors. *Acta Crystallogr. Sect. A 34*, 827–828.

Kantrowitz, E.R. & Lipscomb, W.N. (1988). *Escherichia coli* aspartate transcarbamylase. The relationship between structure and function. *Science 241*, 669–674.

Keller, P.J. & Cori, G.T. (1953). Enzymic conversion of phosphorylase to phosphorylase a. *Biochim. Biophys. Acta 242*, 235–238.

Lee, B. & Richards, F.M. (1971). The interpretation of protein structure: Estimations of static accessibility. *J. Mol. Biol. 55*, 379–400.

Leonidas, D.D., Oikonomakos, N.G., Papageorgiou, A.C., Xenakis, A., Cazianis, C.T., & Bem, F. (1990). Sulphate activates phosphorylase *b* by binding to the Ser-P site. *FEBS Lett. 262*, 23–27.

Lesk, A.M. & Chothia, C. (1984). Mechanisms of domain closure in proteins. *J. Mol. Biol. 174*, 175–191.

Madsen, N.B. (1986). Glycogen phosphorylase: Control by phosphorylation. In *The Enzymes*, 3rd Ed., Vol. 17 (Boyer, P.D. & Krebs, E.G., Eds.), pp. 366–394. Academic Press, New York.

Martin, J.L., Johnson, L.N., & Withers, S.G. (1990). Comparison of the binding of glucose and glucose-1-phosphate derivatives to T state glycogen phosphorylase *b*. *Biochemistry 29*, 10745–10757.

Metzger, B.E., Helmreich, E., & Glaser, L. (1967). The mechanism of activation of skeletal muscle phosphorylase *a* by glycogen. *Proc. Natl. Acad. Sci. USA 57*, 994–1001.

Meyer, F., Heilmeyer, L.M.G., Hashke, R.H., & Fischer, E.H. (1970). Control of phosphorylase activity in muscle glycogen particles. *J. Biol. Chem. 245*, 6642–6648.

Miller, S., Lesk, A.M., Janin, J., & Chothia, C. (1987). The accessible surface area and stability of oligomeric proteins. *Nature 328*, 834–836.

Oikonomakos, N.G., Johnson, L.N., Acharya, K.R., Stuart, D.I., Barford, D., Hajdu, J., Varvill, K.M., Melpidou, A.E., Papageorgiou, T., Graves, D.J., & Palm, D. (1987). Pyridoxal phosphate site in glycogen phosphorylase b: Structure in native enzyme and in three derivatives with modified cofactors. *Biochemistry 26*, 8381–8389.

Oikonomakos, N.G., Melpidou, A.E., & Johnson, L.N. (1985). Crystallisation of pig skeletal muscle phosphorylase b. Purification, physical and catalytic characterization. *Biochim. Biophys. Acta 832*, 248–256.

Perutz, M.F. (1987). Hemoglobin. In *Molecular Basis of Blood Diseases* (Stammatoyanopoulos, G., Niehuis, A.W., Leder, P., & Majerus, P.W., Eds.), pp. 127–128. W.B. Saunders Co., Philadelphia.

Phillips, D.C. (1970). In *British Biochemistry Past and Present* (Choolevin, T.W., Ed.), pp. 11–28. Academic Press, New York.

Schirmer, T. & Evans, P.R. (1990). Structural basis of the allosteric behaviour of phosphofructokinase. *Nature 343*, 140–145.

Sotiroudis, T.G., Oikonomakos, N.G., & Evangelopoulos, A.E. (1978). Effect of sulphated polysaccharides and sulphate ions on the AMP-dependent activity of phosphorylase *a*. *Biochem. Biophys. Res. Commun. 90*, 234–239.

Sprang, S.R., Acharya, K.R., Goldsmith, E.J., Stuart, D.I., Varvill, K., Fletterick, R.J., Madsen, N.B., & Johnson, L.N. (1988). Structural changes in glycogen phosphorylase induced by phosphorylation. *Nature 336*, 215–221.

Sprang, S.R. & Fletterick, R.J. (1979). The structure of glycogen phosphorylase *a* at 2.5 Å resolution. *J. Mol. Biol. 131*, 523–551.

Sprang, S.R., Withers, S.G., Goldsmith, E.J., Fletterick, R.J., & Madsen, N.B. (1991). The structural basis for the association of glycogen phosphorylases b by AMP. *Science 254*, 1367–1371.

Wang, J.H. & Graves, D.G. (1963). Effect of ionic strength on the sedimentation of glycogen phosphorylase a. *J. Biol. Chem. 238*, 2386–2389.

Wang, J.H. & Graves, D.J. (1964). The relationship of the dissociation to the catalytic activity of glycogen phosphorylase a. *Biochemistry 3*, 1437–1445.

Wang, J.H., Shonka, M.L., & Graves, D.J. (1965). The effect of glucose on the sedimentation and catalytic activity of glycogen phosphorylase. *Biochim. Biophys. Acta 18*, 131–135.

Weiss, E.R., Kelleher, D.J., Woun, C.W., Soparkar, S., Osawa, S., Heasley, L.E., & Johnson, G.L. (1988). Receptor activation of G-proteins. *FASEB J. 2*, 2841–2848.

Withers, S.G., Madsen, N.B., & Sykes, B.D. (1982). Covalently activated glycogen phosphorylase: A phosphorus-31 nuclear magnetic resonance and ultracentrifugation analysis. *Biochemistry 21*, 6716–6722.

Withers, S.G., Sykes, B.D., Madsen, N.B., & Kasvinsky, P.J. (1979). Identical structural changes induced in glycogen phosphorylase by two non-exclusive inhibitors. *Biochemistry 18*, 5342–5348.

Yarden, Y. & Ullrich, A. (1988). Growth factor receptor tyrosine kinases. *Annu. Rev. Biochem. 57*, 443–478.